Author Manuscript

Author Manuscript

Author Manuscript

Author Manuscript

HHS Public Access

Author manuscript

Sci Signal. Author manuscript; available in PMC 2023 December 01.

Published in final edited form as:

Sci Signal. 2023 September 26; 16(804): eabq5096. doi:10.1126/scisignal.abq5096.

B cell responses to membrane-presented antigens require the function of the mechanosensitive cation channel Piezo1

Kihyuck Kwak[1,2,†], **Haewon Sohn**[1,†], **Rachel George**[1], **Charles Torgbor**[1], **Javier Manzella-Lapeira**[1], **Joseph Brzostowski**[1], **Susan K. Pierce**[1,*]

[1]Laboratory of Immunogenetics, National Institute of Allergy and Infectious Diseases, National Institutes of Health, Rockville, MD 20852, USA.

[2]Department of Microbiology and Immunology, Institute for Immunology and Immunological Diseases, Brain Korea 21 PLUS Project for Medical Science, Yonsei University College of Medicine, Seoul 03722, Korea.

Abstract

The demand for a vaccine for coronavirus disease 2019 (COVID-19) highlighted gaps in our understanding of the requirements for B cell responses to antigens, particularly to membrane-presented antigens, as occurs in vivo. We discovered that human B cell responses to membrane-presented antigens required the function of Piezo1, a plasma membrane mechanosensitive cation channel. Simply making contact with a glass probe induced calcium (Ca^{2+}) fluxes in B cells that were blocked by the Piezo1 inhibitor GsMTx4. When placed on glass surfaces, the plasma membrane tension of B cells increased, which stimulated Ca^{2+} influx and spreading of B cells over the glass surface, which was blocked by the Piezo1 inhibitor OB-1. B cell responses to membrane-presented antigens but not to soluble antigens were inhibited both by Piezo1 inhibitors and by siRNA-mediated knockdown of Piezo1. Thus, the activation of Piezo1 defines an essential event in B cell activation to membrane-presented antigens that may be exploited to improve the efficacy of vaccines.

INTRODUCTION

B cell activation is initiated by the binding of antigens to the B cell receptor (BCR), which results in the clustering of BCRs, the rapid tyrosine-phosphorylation of BCR cytoplasmic domains, and the recruitment of a number of signaling molecules to form a structure termed a signalosome (1–4). It is becoming increasingly evident that even though B cells respond

*Corresponding author: spierce@nih.gov.
†These authors contributed equally to this work.

Author contributions: Conceptualization: S.K.P., H.S., and K.K. Methodology: H.S., R.G., K.K., C.T., J.B., and J.M.-L. Investigation: H.S., R.G., K.K., C.T., J.B., and J.M.-L. Resources: J.B. and J.M.-L. Software: J.M.-L. Funding acquisition and Supervision: S.K.P. Writing – original draft: S.K.P., H.S., and R.G. Writing – review & editing: K.K.

Competing interests: The authors declare that they have no competing interests.

Data and materials availability: All data needed to evaluate the conclusions in the paper are present in the paper or the Supplementary Materials.

Supplementary Materials
Figs. S1 to S4.
Movies S1 to S5.

Author Manuscript Author Manuscript Author Manuscript Author Manuscript

to both soluble and membrane-presented antigens in vitro, the primary mode of antigen recognition in vivo appears to be of antigens on the surfaces of antigen-presenting cells (APCs) (1, 5, 6). B cell responses to membrane-associated antigens are highly dynamic, involving marked shape changes in the B cells that are controlled by the actin cytoskeleton (7, 8). B cells encountering membrane-associated antigens first rapidly spread over the membrane surface, promoting antigen binding, the formation of signaling-active BCR microclusters, and B cell activation (1, 9, 10). The BCR-antigen microclusters subsequently gathered in the center of the contact area between the B cell and the antigen-containing membrane form a highly complex structure termed an immune synapse. The immune synapse selectively concentrates various B cell coreceptors and membrane structures and excludes others, enabling regulation of BCR signaling (11).

It is now clear that the requirements for activation of B cells by soluble versus membrane-presented antigens are not identical. For example, the B cell coreceptor, CD19, is essential for the responses of B cells to membrane-associated antigens but not to soluble antigens. CD19 transiently associates with BCR microclusters in the immune synapse that form in response to membrane-associated antigens and it stimulates enhanced BCR signaling (12). Moreover, the outcomes of B cell responses to soluble versus membrane-associated antigens can differ (1). We previously reported that B cells of the interferon-γ (IFN-γ)–induced lineage, termed atypical B cells (ABCs), which are greatly increased in number in various chronic infectious diseases and in autoimmune diseases, are unable to respond to soluble antigens (13) but show robust BCR signaling in response to membrane-presented antigens (14). The ability of the ABCs to respond was due in part to the segregation of the inhibitory receptor, FcγRIIb, from the BCR-containing immune synapse after engagement with membrane-bound antigen (14). Thus, the mechanisms underlying the response to membrane-associated antigens appear to be qualitatively different from those underlying responses to soluble antigens and may contribute to substantially different outcomes.

Descriptions of B cell responses in specialized microenvironments in B cell follicles in secondary lymphoid organs provided additional important insights into the roles of the form of the antigen and the physical features of presenting cell membranes in B cell activation (1). Even though B cells encounter low-molecular weight, soluble antigens that flow into follicles through conduits, it appears that antigen encounter by B cells in vivo is primarily with larger antigens captured on the surfaces of APCs and actively trafficked to B cell follicles (5), including by subcapsular sinus macrophages (SCSMs), dendritic cells (DCs), B cells, and follicular dendritic cells (FDCs). Importantly, membrane-presentation of antigens appears to play an important function in affinity selection. The stiffness or flexibility of the APC membrane determines the B cell's affinity threshold for extraction of the antigen, with the soft antigen-presenting membranes of DCs and macrophages enabling antigen extraction by low-affinity, naïve B cells, and the stiff membranes of FDCs imparting a high-affinity threshold for the activation of germinal center (GC) B cells (15).

The observation that the primary mode of antigen recognition by B cells in vivo is of antigen on the surfaces of APCs suggests that B cells can sense differences between antigens in solution versus those presented on cell membranes, possibly through mechanosensitive mechanisms that convert mechanical forces into biological signals. The identification of

Author Manuscript Author Manuscript Author Manuscript Author Manuscript

families of mechanosensitive ion channels, such as Piezo channels (16), has revealed unanticipated roles for mechanical force sensors in important physiological functions in vivo (17). For Piezo channels, these include touch, developmental processes, such as stem cell differentiation, and regulatory processes, including cell migration (17). In the immune system, monocytes depend on Piezo1 to sense lung pressure in response to infections (18); in a mouse model of multiple sclerosis, Piezo1 selectively restrains regulatory T (T_{reg}) cells without affecting effector T_H cell activation or effector functions (19); T cell activation in response to fluid shear stress (20) and T cell receptor (TCR) signaling (21) are enhanced by Piezo1; and Piezo1 is necessary for the development of lymphatic structures (22). Piezo channels are large, trimeric membrane proteins with a three-blade propeller architecture in the plasma membrane and an extracellular cap domain above the central pore that appears to play an important role in channel inactivation. Piezo channels appear to sense or induce membrane curvature through their unusually large number of transmembrane helices. Cryo–electron microscopy (cryo-EM) structures have provided important clues as to the mechanism underlying Piezo channel mechanosensitivity, giving rise to several models, including the force-from-lipid model and the force-from-tether model (17).

Consistent with a possible role for Piezo channels in B cell activation by membrane-presented antigens, *PIEZO1* mRNA, but not *PIEZO2* mRNA, was found in human B cells by Affymetrix microarray (23). Here, we provide evidence that when simply touched by a glass probe in vitro, B cells fluxed Ca^{2+} in a Piezo1-dependent fashion. When placed on glass surfaces, the tension in the B cell plasma membrane increased and the B cells spread over the surface and fluxed Ca^{2+} in an antigen-independent manner, but one that required Piezo1. Critically, B cell responses to membrane-associated antigens, including BCR recruitment to the immune synapse, Ca^{2+} influxes, cell surface expression of the activation marker CD69, actin cytoskeletal rearrangements, and cellular proliferation were blocked by the Piezo1 inhibitors OB-1 (24) and GsMTx4 (25) and by siRNA-mediated knockdown of Piezo1. Thus, Piezo1-dependent Ca^{2+} influx appears to be a previously uncharacterized feature of B cell engagement with membrane-presented antigens that enables B cells to distinguish them from soluble antigens.

RESULTS

Contact with rigid surfaces induces B cells to flux Ca^{2+}

To determine whether B cells sense mechanical forces independently of the BCR, we placed human B cells freshly obtained from peripheral blood and preloaded with the Ca^{2+} indicator dye, CAL520, in a glass chamber. At resting state, B cells adhering to glass showed residual basal Ca^{2+} abundance (Fig. 1A). We then touched the B cells with a glass probe with a 1-μm polished tip and imaged the cells by confocal microscopy. We observed that making contact with the B cells resulted in an immediate, brief Ca^{2+} response that reached a maximum of two- to three-fold the basal signal (Fig. 1A and movie S1). The cells did not show signs of damage when touched by the probe and remained sensitive to touch as demonstrated by their response to subsequent contacts. To determine whether this Ca^{2+} flux was dependent on Piezo1, we repeated the experiment in the presence of a Piezo1 inhibitor, GsMTx4, a spider venom amphipathic peptide toxin that is suggested to inhibit mechanosensitive

Author Manuscript Author Manuscript Author Manuscript Author Manuscript

channels, in part, by binding to and penetrating the outer leaflet of membrane bilayers under tension, resulting in a partial relaxation of the tension rather than binding specifically to Piezo proteins (25). We found that GsMTx4 blocked the influx of Ca^{2+}in B cells touched by the glass probe (Fig. 1A and movie S2), providing evidence of a role for Piezo1 in B cell responses to touch.

To further explore the role of Piezo1 in B cell responses to touch, we placed a purified population of human tonsillar B cells [containing both naïve B cells and memory B cells) (fig. S1)] labelled with CAL520 on glass surfaces and immediately imaged the cells beginning within 15 s as they touched and actively spread over the glass surface. We measured both Ca^{2+}fluxes and B cell spreading over time by total internal reflection fluorescence microscopy (TIRFM) (Fig. 1B). As a control we imaged the dynamics of Ca^{2+}flux in B cells placed on planar lipid bilayers (PLBs) that do not induce B cell spreading (Fig. 1B) (26). Maximal Ca^{2+} fluxes were quantified for B cells placed either on PLB or glass (Fig. 1B). B cells placed on PLB alone did not flatten on the PLB surface or spread over the PLB and did not flux Ca^{2+} (Fig. 1B and movie S3). In contrast, B cells placed on glass surfaces rapidly flattened and spread over the surface and fluxed Ca^{2+}, the magnitude of which increased with time. Similarly, the contact area of B cells placed on glass surfaces but not on PLB increased with time. Plotting the maximal Ca^{2+} increases in B cells placed on glass versus PLB showed considerably increased Ca^{2+} fluxes for the B cells on glass (Fig. 1B, right). To determine whether the Ca^{2+}flux observed for B cells placed on glass was dependent on Piezo1, we repeated the experiment in the presence of OB-1, a small-molecule inhibitor of stomatin-like protein 3, which is required for normal mechanoreceptor function (24). OB-1 blocked the influx of $Ca^{2+}$by B cells placed on glass and significantly reduced the maximal area of B cells spread on glass (Fig. 1C and movie S4). We concluded that B cells flux Ca^{2+}in response to touch through an antigen-independent but Piezo1-dependent mechanism.

To confirm that the B cell Ca^{2+}fluxes in response to touch were antigen-independent and therefore were not influenced by the BCR, we performed the same experiment with purified populations of Ramos cells (a human B cell line) that were either negative for BCR (BCR^- cells) or were stably transduced with plasmids encoding exogeneous immunoglobulin (Ig) heavy (H) and light (L) chains (Trans BCR^+ cells), but expressed similar amounts of Piezo1 (fig. S2). We found that Ca^{2+} fluxes were induced similarly in both BCR^- and Trans BCR^+ Ramos cells (Fig. 1D). Together, these results provide evidence that B cells flux $Ca^{2+}$by a Piezo1-dependent mechanism when sensing mechanical forces provided by either a glass probe or by contact with a glass surface independently of BCR engagement by antigen.

B cell contact with glass surfaces stimulates an increase in plasma membrane tension

Piezo1 opens upon direct physical deformation of the lipid bilayer (16) caused, for example, by changes in membrane tension (27–29). To determine whether B cells placed on glass versus PLB showed increased plasma membrane tension, we purified human tonsil naïve B cells and memory B cells (fig. S1) and labeled them with Flipper-TR, a membrane tension reporter, and then measured changes in tension with fluorescence lifetime imaging microscopy (FLIM) (30, 31). Flipper-TR intercalates into the plasma membrane lipids and,

Author Manuscript Author Manuscript Author Manuscript Author Manuscript

under low membrane tension, the lifetime of the fluorescence probe is short in contrast to the longer lifetime of the probe in membranes under tension (Fig. 2A). We then performed fluorescence imaging of cells placed on PLB or glass in the presence or absence of OB-1 (Fig. 2B) and determined the mean fluorescence lifetimes for a large number of cells (excluding $CD10^+$ GC B cells present in the tonsil preparation) from the analysis (Fig. 2C). The lifetime of the Flipper-TR probe was significantly longer for B cells placed on glass than for B cells placed on PLB, consistent with the observation that B cells placed on glass but not on PLB exhibited a Piezo1-dependent Ca^{2+} flux (Fig. 1B). Note that plasma membrane tension increased in B cells placed on glass even in the presence of OB-1 (Fig. 2C). This observation provided evidence that Piezo1 channel function does not induce plasma membrane tension but rather that increased plasma membrane tension triggered by B cells touching glass surfaces resulted in Piezo activation.

The B cell Ca^{2+} flux in response to the Piezo1 agonist Yoda1 is blocked by siRNA-mediated knockdown of Piezo1

Thus far, the function of Piezo1 in B cell responses to touch was inferred by blocking these responses with the Piezo1 inhibitors, GsMTx4 and OB-1 (Figs. 1 and 2). We next investigated whether reducing the abundance of Piezo1 in B cells directly affected the B cell Ca^{2+} response to the Piezo1 agonist, Yoda1 (19, 32). Yoda1 is a soluble allosteric agonist of Piezo1 that appears to act as a molecular wedge upon binding to Piezo1, resulting in persistent Piezo1 opening (33). We measured Ca^{2+} influxes in B cells over 15 min in response to Yoda1 and determined the average fold-change in Ca^{2+} influx across multiple experiments (Fig. 3A). To reduce Piezo1 abundance, human peripheral blood B cells were transfected with either a control siRNA or a Piezo1-specific siRNA. The siRNA used for the transfection was chosen because it was used in the original study that described Piezo1 as an essential component of distinct mechanically activated ion channels in which the maximal knockdown of Piezo1 of ~50% was sufficient to specifically reduce mechanically activated cation channel activity (16). The protocol used to obtain the highest transfection efficiency was optimized by monitoring transfection efficiency with siGlo-Red, an siRNA substitute (fig. S3A). We measured the amount of *PIEZO1* mRNA relative to that of *GAPDH* mRNA by qRT-PCR analysis and also measured Peizo1 protein by flow cytometry with a Piezo1-specific antibody (Fig. 3B). Relative to that in cells transfected with the control siRNA, the abundance of Piezo1 mRNA and protein in cells transfected with Piezo1-specific siRNA (Piezo1-KD cells) was reduced by 50%.

We measured Ca^{2+}fluxes in control and Piezo1-KD B cells in solution in response to Yoda1 (Fig. 3C, fig. S3B). The Ca^{2+}influx in response to Yoda1 was reduced in the Piezo1-KD cells as compared to that in control cells (Fig. 3C). In contrast, responses to anti-Ig and ionomycin were similar for control and Piezo1-KD cells (Fig. 3D). We also determined whether membrane tension increased in control and Piezo1-KD cells placed on glass surfaces as an independent measure of Piezo1 activity. As compared to that in control B cells, the fluorescence lifetime of Flipper-TR was significantly reduced in Piezo1-KD cells (Fig. 3E). Thus, the correlation of reduced Piezo1 abundance with reduced cellular responses to Yoda1 and to glass surfaces provides evidence that Piezo1 is required for Ca^{2+}fluxes under these conditions.

Author Manuscript Author Manuscript Author Manuscript Author Manuscript

The B cell Ca^{2+} responses to Yoda1 and to BCR crosslinking are independent

Crosslinking of the BCR by anti-Ig results in the phosphorylation of the BCR and assembly of a signalosome that stimulates PLCγ-dependent Ca^{2+} fluxes. Our earlier experiments (Fig. 1D) showed that the presence of the BCR on B cell surfaces was not required for the Ca^{2+} influx induced by placing the cells on a glass surface. To explore the relationship between B cell Piezo1-dependent Ca^{2+}responses to touch and B cell responses to BCR crosslinking, we determined the effect of Yoda1 on the response of human tonsillar naïve B cells and memory B cells to BCR crosslinking by soluble anti-Ig in vitro when Yoda1 was added before, at the same time as, or after BCR crosslinking by anti-Ig (Fig. 4A). In each case, the Ca^{2+}response was quenched by the addition of the Ca^{2+}chelator EGTA. The addition of Yoda1 to B cells induced Ca^{2+}influx that persisted until subsequent BCR crosslinking induced an additional transient Ca^{2+}peak that then returned to that induced by Yoda1 alone. The simultaneous addition of Yoda1 and anti-Ig resulted in an initial transient Ca^{2+}influx (~200 sec) of the same magnitude as the Ca^{2+}peaks induced by Yoda1 followed by anti-Ig, which subsequently returned to that induced by Yoda1 alone. The addition of anti-Ig before Yoda1 resulted in a small transient Ca^{2+}influx that returned to near basal signal before the subsequent addition of Yoda1 induced a persistent Ca^{2+}influx of a magnitude similar to that observed when Yoda1 was provided before or together with anti-Ig. Together, these results are consistent with B cells in solution mounting independent responses to BCR crosslinking and to Piezo1 activation that appeared additive in the presence of both anti-Ig and Yoda1, regardless of the order of addition.

We further explored the BCR-independence of the Yoda-induced Ca^{2+}responses in cells by assessing the response to Yoda1 of Ramos cells that either were BCR^{-}, expressed an endogenous BCR (Endo BCR^{+} cells), or stably expressed exogenous IgH and IgL chain (Trans BCR^{+}) (fig. S2). Piezo1 abundance was similar in all three B cell lines (fig. S2). The Ca^{2+}responses of the three Ramos cell populations to Yoda1 and to ionomycin as a control were not significantly different, suggesting that the expression of a BCR did not have a measurable effect on the response to Yoda1 (Fig. 4B). In addition, the response of the BCR^{+} Ramos cells to Yoda1 was not affected by the presence of an inhibitor of the essential early BCR kinase, Syk (Fig. 4C), whereas the Syk inhibitor blocked the response of BCR^{+} Ramos cells to BCR crosslinking with anti-Ig (Fig. 4D). These results provide additional evidence that B cells flux Ca^{2+} in response to the agonist Yoda1 in a manner independent of BCR signaling.

BCR-induced B cell activation by membrane-associated anti-Ig but not by soluble anti-Ig requires Piezo1

To determine whether B cell responses to soluble or membrane-associated antigens were dependent on Piezo1 activity, we purified naïve IgM^{+} human tonsillar B cells, labeled them with fluorescent Fab human Igμ-specific antibodies (Fab anti-IgM) to visualize the BCR, and placed them on PLB alone or on PLB to which human Ig-specific antibodies (anti-Ig) were attached to mimic membrane-presented antigen-crosslinking of the BCR as previously described (34). Contact of the B cells with the PLB for 25 min at 37°C in the presence or absence of the Piezo1 inhibitor, OB-1, was imaged by TIRFM. In addition to collecting TIRFM images of individual B cells. we also quantified the total fluorescence

Author Manuscript Author Manuscript Author Manuscript Author Manuscript

intensity (TFI) of the BCR in the area of contact with the PLB (Fig. 5A). B cells placed on PLB-anti-Ig accumulated BCR in the area of contact between the B cell and the PLB-anti-Ig, which was blocked by OB-1, suggesting that BCR accumulation in the contact area was dependent on the activity of Piezo1. We also observed that a small amount of BCR appeared in the contact area of the B cell with PLB alone and that this accumulation was blocked by the inhibitor OB-1. We previously reported antigen-independent weak polarization of BCRs and cell-scaffolding structures similar to the polarization observed here (35). The result here suggests that OB-1 blocks both antigen-independent and antigen-dependent BCR accumulation in the contact area.

We also tested several additional active compounds for their effects on the responses of human tonsillar IgM^+ and IgG^+ naïve and memory B cells to PLB-anti-Ig (Fig. 5B). We observed that OB-1, EGTA, GsMTx4, and a Syk inhibitor significantly reduced BCR accumulation in the contact area with the PLB-anti-Ig as compared to that in the untreated control, consistent with a requirement for Piezo1 activation in the antigen-driven formation of an immune synapse. We also observed weak accumulation of the BCR in the contact area of the B cell with PLB alone, but for this mixed population of IgM- and IgG-expressing naïve and memory B cells, only GsMTx4, but not OB-1, reduced BCR accumulation. Additional studies are planned to address the requirements for Piezo1 in human B cells of different subtypes.

We next used confocal microscopy to measure the influx of Ca^{2+} into B cells in response to either PLB-anti-Ig or soluble anti-Ig after pretreatment with OB-1 or buffer alone. B cells placed on PLB-anti-Ig showed peak Ca^{2+} influx by 1 min that gradually decreased, reaching basal amounts by 13 min (Fig. 5C). In OB-1–pretreated B cells, Ca^{2+} influx was blocked. In contrast, pretreatment with OB-1 did not have a significant effect on the magnitude of Ca^{2+} influx induced by soluble anti-Ig, although OB-1 appeared to delay the peak Ca^{2+} responses to soluble anti-Ig (Fig. 5C).

We also investigated the requirement for Piezo1 in BCR-induced increases in the expression of the cell surface activation marker, CD69 (36), in response to PLB-anti-Ig versus soluble anti-Ig. Naïve human tonsillar B cells were either placed on PLB-anti-Ig or incubated with anti-Ig in solution for 24 hours in the presence or absence of OB-1. Cells were collected and CD69 surface expression was quantified by flow cytometry and expressed as the ratio of fluorescence intensity for anti-Ig alone and anti-Ig in the presence of OB-1. A ratio of 1 indicated no effect of OB-1 on CD69 expression; a ratio >1 indicated that OB-1 inhibited CD69 expression, whereas a ratio <1 indicated that OB-1 led to increased CD69 expression. We found that OB-1 inhibited membrane-associated anti-Ig from inducing CD69 expression on B cells (ratio >1) but had no effect on the ability of soluble anti-Ig to stimulate B cell CD69 expression (ratio = 1) (Fig. 5D). We also found that the Piezo1 inhibitor GsMTx4 blocked increases in CD69 expression on B cells in response to PLB anti-Ig but had little effect on the response to soluble anti-Ig (Fig. 5E). Together these results provide evidence that Piezo1 is required for B cell activation by membrane-presented anti-Ig but not for B cell responses to soluble anti-Ig.

Author Manuscript Author Manuscript Author Manuscript Author Manuscript

B cell responses to membrane-presented anti-Ig require Piezo1

From our earlier results, the requirement of Piezo1 in B cell responses to membrane-associated anti-Ig was based on the inhibitory effects of the Piezo1 inhibitors OB-1 and GsMTx4. To provide direct evidence for the role of Piezo1 in B cell responses to membrane-associated anti-Ig, we used TIRFM to compare the responses of control and Piezo1-KD cells to PLB alone or PLB-anti-Ig with respect to Ca^{2+} fluxes and the area of contact between the cells and the PLB. We found that control and Piezo1-KD cells did not spread or flux Ca^{2+} when placed on PLB alone; however, when placed on PLB-anti-Ig, control cells both spread and fluxed Ca^{2+} (Fig. 6, A and B, movie S5). In contrast, Ca^{2+} fluxes and cell spreading were not exhibited by Piezo1-KD cells (Fig 6, A and B, Movie S5).

We also measured the accumulation of BCR in the contact area with the PLB-anti-Ig and the degree of actin polymerization in control and Piezo1-KD cells placed on PLB-anti-Ig for up to 10 min. We found that the relative abundances of the BCR and total F-actin were similar in control and Piezo1-KD cells (fig. S4). Control cells accumulated considerably more BCR in the contact area as compared to Piezo1-KD cells placed on PLB alone (Fig. 6C), and maximal BCR accumulation was reached after 5 min and persisted until 10 min. In contrast, Piezo1-KD cells did not accumulate more BCRs in the contact area than was accumulated by cells placed on PLB alone until 7.5 min and that amount increased further by 10 min (Fig. 6C). Thus, Piezo1 appears to facilitate the rapid, stable accumulation of BCRs in the immune synapse. Consistent with this observation, the Piezo1-KD cells showed reduced accumulation of both BCRs and F-actin at the immune synapse as compared to control B cells. In addition, the characteristic dynamics of actin polymerization, in which F-actin increases, reaching a maximum before decreasing as the immune synapse forms (as was observed for control B cells) (8) were not exhibited by Piezo1-KD cells (Fig. 6C). Together, these results suggest that Piezo1 expression is necessary for the rapid and stable accumulation of BCRs at the immune synapse, as well as for actin polymerization in response to membrane-associated anti-Ig. We also investigated the proliferative responses of control and Piezo1-KD cells to PLB-anti-Ig alone or in the presence of anti-CD40 monoclonal antibody, IL-4, and IL-21 (helper T cell medium) to mimic T cell help (Fig. 6D). The proliferation of Piezo1-KD cells was considerably less than that of control B cells, providing additional evidence for a role of Piezo1 in driving antigen-specific responses in B cells.

DISCUSSION

Although it is well-established that B cells respond to antigens present in solution and to antigens presented on membranes in vitro, B cells appear to strongly favor membrane-presented antigens in vivo. Here, we provided evidence for a possible mechanism for this preference. We showed that BCR-dependent B cell activation was preceded by the B cell sensing its contact with a solid surface through the activation of its plasma membrane mechanosensing Ca^{2+} channel, Piezo1. Piezo1 is a member of a mechanosensitive ion channel family that, like all members of mechanically activated ion channel families, enables cells to convert mechanical stimuli into chemical signals (16). For these channels, tension-induced changes in free energy overcome the stability of the channel in its closed state,

Author Manuscript Author Manuscript Author Manuscript Author Manuscript

resulting in channel opening (37–39). Piezo1 appears to be inherently mechanosensitive, and its activation fits the “force-from-lipid” model (29), in which the changes in the tension of the plasma membrane are directly converted into expansion of the mechanosensitive channel without the requirement for additional elements, including the actin cytoskeleton (40). Thus, Piezo1 reconstituted in planar membranes undergoes substantial expansion when tension is applied to the membrane (29).

Here, we described a process in which contact with a solid surface perturbs the plasma membrane of the B cell, resulting in an increase in plasma membrane tension sufficient to activate Piezo1, enabling Ca^{2+} influx. The Ca^{2+} influx induced by Piezo1 activation appeared to be independent of that induced by BCR crosslinking. Although Piezo1 can be activated to enable Ca^{2+} influx into B cells in solution by treatment with the small-molecule Piezo1-specific agonist, Yoda1, in our studies, we found no evidence that BCR crosslinking of B cells in solution affected Yoda1-mediated Piezo1 activation or that, once activated by Yoda1, Piezo1 affected BCR crosslinking–induced BCR signaling. Rather, we observed that B cell responses to BCR-crosslinking in solution, including Ca^{2+} influx and induction of the cell surface expression of the activation marker CD69, were not affected by Piezo1 inhibition. In addition, we showed that for B cells in solution, Piezo1 activation by Yoda1 and BCR crosslinking independently triggered Ca^{2+} fluxes, suggesting that Piezo1 did not function to regulate BCR-induced Ca^{2+} influxes directly. Even though we found no evidence that Piezo1 activation in B cells in solution affected BCR-induced signaling, we would not rule out the possibility that in response to membrane-associated antigens Piezo1-mediated Ca^{2+} fluxes may activate cellular circuits that influence subsequent BCR functions induced by membrane-associated antigens. Many differences in the mechanisms by which B cells respond to membrane-associated antigens versus soluble antigens have been described, and it is possible that such differences are the result of Piezo1-regulated processes. These include: antigen valency [B cells in solution respond only to multivalent antigens, whereas B cells readily respond to monovalent antigens associated with membranes (41)]; the cellular architecture associated with BCR signaling [B cells in solution form relatively simple BCR-antigen microclusters (42) in contrast to the complex immune synapse formed by B cells in response to membrane-associated antigens (8, 9)]; and the requirement for coreceptors in the immune synapse (CD19 is required for responses to membrane-associated, but not soluble, antigens (12)]. It will be important to better understand such connections to fully exploit Piezo1 function in the design of vaccines.

The results presented here offer a mechanism that may explain, in part, why B cell activation in vivo is predominantly in response to membrane-presented antigens. We speculate that the preference for membrane-presented antigens may have been evolutionarily acquired to focus B cell responses on particulate pathogens and their antigens. Such antigens have the propensity to form immune complexes or fix complement, enabling their presentation by Fc receptor– and complement receptor–expressing APCs in secondary lymphoid tissues, a property that is lacking for small, soluble self-antigens that enter B cell follicles through conduits. In a sense, Piezo1 may play a similar role to that of innate receptors that alert B cells to the presence of dangerous pathogens through the recognition of pattern-associated molecular patterns (PAMPs). For Piezo1, the PAMP may be a quality of the pathogen that can exert tension on the B cell plasma membrane. The results presented here also suggest

Author Manuscript Author Manuscript Author Manuscript Author Manuscript

that designing vaccines that can exert tension on the plasma membrane of B cells and activate Piezo1 may greatly improve their efficacy. Indeed, some virus-like particles (VLPs) have proven to be effective vaccines (43), and considerable effort is being made toward exploring the structural features of VLPs that account for their potency as vaccines.

Concerning the possible function of Piezo1 in B cell activation, it is of interest that approximately one third of populations in malaria-endemic Africa carry a *Piezo1* gain-of-function mutation (E756del) (44). The high frequency of this gain-of-function allele in malaria-endemic Africa suggests that it is likely under malaria-selective pressure. Indeed, red blood cells from individuals carrying the E756del allele are resistant to infection by *Plasmodium falciparum* parasites in vitro. Antibodies play a critical role in immunity to malaria, but acquisition of protective antibodies is remarkably slow, requiring years of parasite exposure, which leaves children susceptible to severe malaria and death (45). It is possible that an increase in Piezo1 function in B cells responding to membrane-associated antigens could have a deleterious effect and contribute to the slow acquisition of immunity in Africans carrying the E756del allele.

Studies have highlighted a potential role for Piezo1 in the regulation of innate immune cells (18) and T cells (19). In monocytes and monocyte-derived macrophages, Piezo1 plays a role in initiating inflammatory responses in vitro through its response to cyclical hydrostatic pressure similar to that experienced by immune cells in the lung. Piezo1 is also critical for the response to bacterial infection in the lung. Piezo1-deficient monocytes are recruited to the infected lung but do not attract neutrophils (18). In mouse models of multiple sclerosis, deletion of *Piezo1* in T cells results in an expanded population of T_{reg} cells and attenuation of disease (19). It will be of interest to elucidate the mechanisms that alter plasma membrane tension in these immune cells to activate Piezo1 and Ca^{2+} flux, and how Ca^{2+} is linked to the biological outcomes of the response. Looking toward the future, it will be critical to develop the genetic mouse models to enable study of the function of Piezo1 in vivo. Key questions remain concerning the role of Piezo in B cell development and tolerance and at different differentiated stages, as well as in B cell responses in lymphoid tissues to antigen challenge and infections. It will also be critical to better understand the requirement of Piezo1 function in human B cells in driving the fates of long-lived plasma cells and memory B cells. Such studies of Piezo1 function in human B cell responses to vaccines are feasible in vitro. Of particular interest are requirements for Piezo1 in response to vaccines designed to mimic infectious pathogens, in particular VLP-based vaccines. In summary, our results provide insights into mechanosensing mechanisms that may account, at least in part, for the well-established phenomenon that B cell responses to membrane-presented antigens versus soluble antigens have different cellular requirements and often lead to different outcomes. An important question remains: will it be possible to harness this mechanosensing mechanism to drive the desired outcome of BCR-dependent B cell responses in the design of vaccines and therapies?

Author Manuscript Author Manuscript Author Manuscript Author Manuscript

Materials and Methods

Human tonsil and peripheral blood samples

Fresh buffy coats or leukapheresis samples were obtained from healthy individuals enrolled at the National Institutes of Health (NIH). Informed consent was obtained from all participants. Fresh human tonsils were obtained from patients undergoing tonsillectomies at the pathology department of Children's National Medical Center, Washington, DC. Use of these tonsils for this study was exempted from review by the NIH Institutional Review Board in accordance with the guidelines issued by the Office of Human Research Protections. The demographics of the sample donors were not collected for this research.

Cell line and cell culture

The human Burkitt lymphoma B cell line Ramos.2G6.4C10 (ATCC, CRL-1923, CVCL_1646) and the human T lymphoblast cell line Jurkat (Clone E6-1, CVCL_0065) were grown in complete medium, which contains RPMI 1640 medium (11875-093), 2-Mercaptoethanol (55 μM, 21985-023), Penicillin-Streptomycin (100 U/mL, 15140148), Sodium pyruvate (1 mM, 11360-070), and MEM Non-Essential Amino Acid (1:100, 11140-050) from Gibco and 10 mM HEPES (Quality Biological, 118-089-721), supplemented with 10% fetal bovine serum (FBS, Gibco, 26140079).

Primary B cell isolation from human tonsils and peripheral blood samples

Single-cell suspensions of human tonsillar B cells were prepared by mechanical disruption and negative selection with the EasySep Human B cell enrichment kit (STEMCELL technology, 19054) (46). Human peripheral blood B cell isolation from buffy coats or leukopaks required the EasySep Direct Human B cell isolation kit (STEMCELL technology, 19674) or PBMC separation by density gradient with Ficoll-Paque Plus (cytiva, 17144002), which was followed by B cell isolation with an EasySep Human B cell enrichment kit. The purity of the B cells was > 95%. Freshly isolated primary B cells were used for all experiments.

Antibodies and reagents

For Piezo1 function studies, Yoda 1 (5586), GsMTx4 (4912), and OB-1 (6545) were obtained from Tocris Bioscience. The Syk inhibitor P505-15 hydrochloride (9583-5) was obtained from BioVision. The Ca^{2+} indicator dye, CAL520, sodium salt (AAT Bioquest, 21135), ionomycin, calcium salt (Tocris, 1704), 0.5 M EGTA solution (bioWorld, 40520008-1), and the red fluorescence dye, CellTrace Far Red cell proliferation kit (Invitrogen, C34564) as a cell volume sensor were used for Ca^{2+} assays by either flow cytometry or live-cell imaging. Flipper-TR (Spirochrome AG, SC020) was used for FLIM. For flow cytometry, the following antibodies were used: anti-human CD10-BV421 (312217), CD27-BV421 (124223), and CD69-PE (310906) were from Biolegend. Anti-Piezo1-Alexa Fluor 647 (Novusbio, NBP1-78446AF647) and anti-rabbit IgG (H+L), $F(ab')_2$ Fragment-Alexa Fluor 647 (Cell Signaling Technology, 4414). Normal goat serum (SouthernBiotech, 0060-01) was used for blocking nonspecific antibody binding. For surface BCR labeling in Ramos cells, goat Fab anti-human Igμ H chain-Alexa Fluor 647 (Jackson

Author Manuscript Author Manuscript Author Manuscript Author Manuscript

ImmunoResearch, 109-607-043) for H chain and anti-human Igκ-PE (BD Biosciences, 555792) for Igκ L chain or for κ and λ L chain labeling, unlabeled goat Ig Fab′2 anti-human Kappa (2062-01) and Lambda (2072-01) from Southern Biotech were mixed at 1:1 (goat Ig Fab′2 anti-human κ + λ light chains) and then conjugated with either Alexa Fluor 488 (332-0005) or DyLight 488 (322-0010) with the Lightening-Link Rapid antibody labeling kit (Novusbio), according to the manufacturer's protocol. To isolate BCR^+ Ramos cells by magnetic bead sorting, anti-human Igμ H chain-PE (555783) and Igκ L chain-PE (555792) were from BD Biosciences. LIVE/DEAD Fixable Near IR (780) (L34994) or Violet (L34955) Viability Kits for dead cell exclusion, Phalloidin-Alexa Fluor 647 (A22287) or Phalloidin-Alexa Fluor 488 (A12379) from Invitrogen were used for F-actin staining, the cell proliferation dye eFluor 450 (Invitrogen, 65-0842-85) was used for cell proliferation assays. For surface BCR labeling in imaging experiments, goat pAb Fab anti-human IgG, Fcγ-specific-Alexa Fluor 488 (109-547-008) or Alexa Fluor 647 (109-607-008), anti-human IgM, Fc5μ-specific-Alexa Fluor 488 (109-547-043) or Alexa Fluor 647 (109-607-043) from Jackson ImmunoResearch laboratories and anti-human IgD (34) conjugated with DyLight650 with the Lightening-Link Rapid DyLight650 antibody labeling kit (Novusbio, 326-0010) were used. For BCR crosslinking, either the mouse monoclonal antibody anti-human Kappa (BioRad, 5268-6010) or 1:1 mixed unlabeled goat Ig Fab′2 anti-human Kappa (2062-01) and Lambda (2072-01) and biotin-labeled anti-human Kappa (2062-08) and Lambda (2072-08) from Southern Biotech were used for soluble antigen and for PLB-anti-Ig, respectively. For B cell proliferation assays, the mouse monoclonal antibody anti-human CD40 (Biolegend, 313020), IL-21 (8879-IL) and IL-4 (6507-IL) from R&D were used in the medium mimicking T_H cell (T_H medium).

Ca^{2+} imaging after cell perturbation

To measure the Ca^{2+} response to mechanical touch, human B cells labeled with CAL520 according to the manufacturer's protocol (47) were plated onto MatTek 35-mm round #1.5 cover glass bottom culture dishes (MatTek Corp, P35G-1.5-10-C) in Medium 199 (Gibco, 11043-023) in the absence or presence of 5 μM GsMTx4 for about 10 min before imaging at 37°C on a Zeiss LSM 880 laser-scanning confocal microscope equipped with a 63X, 1.4 NA Plan Apochromatic objective lens (Carl Zeiss Microscopy), a stage top incubator (Okolab), and a TransferMan NK2 micromanipulator (Eppendorf). Cells treated with GsMTx4 were incubated for 45 min at 37°C in 5% CO_2 before plating. Using a custom-made micropipette with a polished 1-μm tip (Sutter Instrument, BR100-10), cells were gently touched proximal to the glass-attached region of the cell near the cell body. The change in fluorescence intensity was monitored at ~2 frames/s with a 488-nm excitation laser and 500 to 550-nm detection wavelength range. The excitation laser power output was set at 0.01%. No photobleaching or cell damage was detected. Fluorescence intensity values were measured with the Zen Blue analysis software package. Fold-changes in fluorescence intensity after background subtraction after the cell was touched is reported.

Transduction of BCR-deficient Ramos cells to express exogenous BCR

A surface IgM–negative clone of Ramos cells (BCR^-) was transduced with lentiviral vectors expressing exogenous human Igμ heavy (H) and κ light (L) chains. BCR^- Ramos cells were purified from Ramos cells through multiple rounds of cell sorting and enrichment

Author Manuscript Author Manuscript Author Manuscript Author Manuscript

by negative selection with anti-human Igμ H chain vs. anti-λ L chain staining (48). The lentiviruses were produced in the Lenti-X 293T cell line after transfection with the FEEKW lentiviral expression system (48). Surface BCR–positive cells, defined as staining for both Igμ H chain and L chain (κ), were purified by positive magnetic bead isolation with the aid of anti-human Igμ-PE and anti-human Igκ-PE and the EasySep Human PE positive selection kit (STEMCELL technologies, 17664) according to the manufacturer's instructions.

Transfection of peripheral B cells with siRNAs

The Amaxa P3 Primary Cell 4D-Nucleofector X Kit (Lonza, NC0301987) and the 4D-Nucleofector X unit (Lonza, Cologne, Germany) were used to transfect isolated peripheral B cells, according to the manufacturer's protocol. To monitor RNA transfection efficiency depending on concentration, siGlo-Red, a small RNA molecule transfection indicator (Horizon Discovery, D-001630-02-05) was used as a substitute for siRNA, and the best transfection condition was predetermined. Freshly isolated peripheral B cells (3×10^6 cells) were transfected with 300 to 400 nM of either the control siRNA, ON-TARGETplus Non-targeting Pool (Dharmacon, D-001810-10-15), or the Piezo1-specific siRNA, ON-TARGETplus Human *PIEZO1* (9780) siRNA-SMARTpool (Dharmacon, L-020870-03-0005). The transfected cells were immediately placed in 6-well plates with complete medium supplemented with 10% FBS and cultured for a minimum of 3 days before functional assays were performed or the abundances of Piezo1 mRNA and protein were determined by qRT-PCR assay and flow cytometry analysis, respectively. Transfected cells were monitored for viability and further tested for the functional loss of Piezo1 by Yoda-1-induced Ca^{2+} flux for use in functional assays by imaging and in cell activation and proliferation assays. Piezo1-KD cells showing a minimum of 40% reduced Ca^{2+} flux compared to that in control cells were used for the functional assays.

Reverse transcription and qRT-PCR

qRT-PCR assays were performed with a QuantStudio 6 Flex Real-Time PCR system (Applied Biosystems), Cells-to-CT 1-Step Taqman Kit (Invitrogen, A25603), and *GAPDH* (NM_002046.3) and *PIEZO1* (Hs00207230_m1) TaqMan Probes (Thermo Fisher). QuantStudio software was used to calculate the cycle threshold number, C_T values, and the relative gene expression of Piezo1-KD samples as compared to that of the control was calculated with the $2^{-\Delta\Delta CT}$ method (49). For the quantification of *PIEZO1* mRNA in Jurkat and Ramos cell lines, RNA from cultured Jurkat cells, BCR negative Ramos (BCR^-) cells, endogenous BCR Ramos (Endo BCR) cells, and BCR^- cells transduced to express exogenous heavy (H) and light (L) chains (Trans BCR) cells, was extracted with the Quick RNA MicroPrep RNA extraction kit (Zymo Research, R1050) according to the manufacturer's instructions and DNase treated. We then synthesized cDNA with a reverse transcription system (Bio-Rad, 1725038). Real-time RT-PCR was performed with triplicate samples with the Bio-Rad CFX connect Real-Time System (Bio-Rad, Hercules). The specific Taqman primer/probe sets (Thermo Fisher Scientific) were human *PIEZO1* (Hs00207230_m1) and human *GAPDH* (Hs99999905_m1). Relative gene expression was calculated with the $2^{-\Delta CT}$ formula.

Author Manuscript Author Manuscript Author Manuscript Author Manuscript

Preparation of planar lipid bilayers

As a surrogate of antigen tethered on APCs, a PLB was used to tether anti-Ig as a model membrane-associated antigen. PLBs were prepared as described previously (51). Briefly, PLBs were prepared in 8- or 18-well chambered cover glass made by nanostrip-cleaned #1.5 cover glass adhered on it with either 8-well Lab-Tek chambered cover glass (Nunc, 155411) replaced for the bottom coverglass or sticky Slide (ibidi, 81818). A working solution of 100 μM small, unilamellar vesicles was prepared from the stock solution, consisting of 1,2-dioleoyl-sn-glycerol-3-phosphocholine (DOPC, 850375) and 1,2-dioleoyl-sn-glycero-3-phosphoethanolamine-N-(cap biotinyl) (DOPE-cap biotin, 870273C) from Avanti Polar Lipids at a ratio of 100:1. To bind anti-Ig to the PLB, the wells containing PLB were incubated at room temperature with streptavidin (2.5 μg/ml) for 10 min, which was followed by incubation with biotinylated goat F(ab′)2 anti-human κ + λ (1 μg/ml) for 20 min with washing between the incubations with PBS.

Flow cytometry

To measure the abundance of total Piezo1 protein in Ramos cell lines, cultured cells were fixed and permeabilized with the BD Cytofix/Cytoperm kit (BD Biosciences, 554714). Cells were either unstained or were incubated with human Piezo1-specific rabbit polyclonal antibodies (1 μg/ml) (50) or a matched isotype control (Cell Signaling Technologies) and Live/Dead Fixable violet, fluorescent reactive dye, followed by a secondary antibody anti-Rabbit IgG (H+L), $F(ab')_2$ fragment conjugated with Alexa Fluor 647. To measure cell surface BCR abundance, cultured Ramos cells were stained with Alexa Fluor 647–conjugated anti-human Igμ H chain and Alexa Fluor 488–conjugated goat Ig Fab′2 anti-human κ + λ L chains or anti-human κ L chain-PE and Live/Dead Fixable violet. Piezo1 and BCR abundances were analyzed as geometric mean fluorescence intensity (gMFI) with FlowJo software. The same Piezo1-specific antibodies were used to measure total Piezo1 protein in control siRNA– and Piezo1-siRNA–transfected peripheral blood B cells after they were fixed with 4% PFA for 20 min, permeabilized with 0.2% Triton-100 for 10 min, and blocked with normal goat serum (1:100 dilution) for 1 hour at room temperature. After overnight incubation with Piezo1 antibodies at 4 °C followed by incubation with secondary goat anti-rabbit IgG-Alexa Fluor 647 antibodies for 30 min at room temperature, flow cytometry was performed. For F-actin staining, siRNA-transfected cells were stained with Phalloidin–Alexa Fluor 647 or Phalloidin–Alexa Fluor 488 after undergoing fixation and permeabilization according to the manufacturer's protocol. Flow cytometry data were analyzed with FlowJo software to obtain median FI values for the quantification of Piezo1 and F-actin in siRNA-transfected B cells. Yoda1- and soluble antigen–induced Ca^{2+} flux assays were performed by flow cytometry. Purified tonsillar B cells were labeled with CAL520 according to the manufacturer's protocol (47), stained with mouse monoclonal anti-human CD10-BV421 and Live/Dead Fixable Near-IR viability dye. To stimulate Piezo1, cells (5×10^6/ml) were treated with 5 μM Yoda1 in Medium199 after 180 s of baseline recording, and data was acquired over 1000 s. For BCR crosslinking, tonsillar B cells were treated with mouse mAb anti- human κ light chain (10 μg/ml), whereas peripheral blood B cells were incubated with goat Ig Fab′2 anti-human κ + λ light chains as a surrogate antigen (anti-Ig). To investigate the relationship between Piezo1- and BCR-induced Ca^{2+} flux when soluble antigen was engaged, 15 μM Yoda1 and anti-Ig were

Author Manuscript Author Manuscript Author Manuscript Author Manuscript

added to cells either sequentially, with a 240 s interval, or simultaneously after 120 s of baseline recording. We then added 2 mM EGTA at 820 s to quench extracellular Ca^{2+}. Naïve and memory B cells ($CD10^{-}$) were analyzed for their Ca^{2+} response to Yoda1, anti-Ig, or both, and were compared with FlowJo software (FlowJo, LLC) and Prism (GraphPad). For peripheral blood B cells transfected with control or Piezo1-specific siRNA, the cells were stained with CAL520, and baseline Ca^{2+} flux was recorded. Yoda1 or anti-Ig was added to the B cells, and Ca^{2+} flux was recorded by flow cytometry. At the end of the recording, ionomycin- was added to the cells, and the resulting Ca^{2+} increase was recorded. Ca^{2+} fluxes were calculated as the fold-change in CAL520 MFI per unit time of the area under the curve (AUC) after stimulation relative to that of baseline, after obtaining the values for the period of baseline ($MFI_{baseline}$), Yoda1 stimulation (MFI_{Yoda1}), anti-Ig stimulation ($MFI_{anti\text{-}Ig}$), ionomycin stimulation ($MFI_{ionomycin}$) from the kinetic Ca^{2+}graph in FlowJo. To measure the cell surface expression of CD69 in the presence of the Piezo1 inhibitors OB-1 and GsMTx4, purified naïve tonsillar B cells were pretreated with 20 μM OB-1 for 1 hour, 5 μM GsMTx4 for 30 min, or were left untreated for 1 hour (control for OB-1) or 30 min (control for GsMTx4) at 37°C and placed into a well coated with either biotinylated goat F(ab′)2 anti-human κ + λ (Southern biotech)-bound PLB (PLB-anti-Ig) or 2 μg/mL biotinylated goat F(ab′)2 anti-human κ + λ in solution (Soluble anti-Ig) in an 18-well, chambered cover glass and cultured in the absence or presence of 20 μM OB-1 or 5 μM GsMTx4 overnight. Cells were harvested, washed with cold PBS, and then stained with fluorescently labeled mouse monoclonal anti-human CD69 on ice for 30 min, and analyzed by flow cytometry to determine the CD69 geoMean FI (OB-1 experiment) or median FI (GsMTx4 experiment) and the ratio of anti-Ig without OB-1 or GsMTx4 over that with OB-1 or GsMTx4 was calculated for PLB-anti-Ig or soluble-anti-Ig stimulation after normalization by the no anti-Ig condition in PLB or solution. into analyze the proliferation of B cells transfected with control or Piezo1-specific siRNAs, the cells were cultured for 24 hours after transfection, labeled with the cell proliferation dye eF450 according to the manufacturer's protocol, and placed in chambers with PLB alone or PLB-anti-Ig in the absence or presence of anti-CD40 antibody (1 μg/ml), IL-21 (100 ng/ml), and IL-4 (25 ng/ml; T_H medium), and cultured for 5 days. Harvested cells from the chambers in each culture condition were stained with LIVE/DEAD Fixable Near IR Viability dye for dead cell exclusion and assayed with an LSRFortessa X20 flow cytometer (BD Bioscience). Data were quantified as the percentage of proliferating cells by gating cells that had a proliferation dye signal that was less than the signal of the dye-labeled cells at day 0, and the ratio of the proliferation of Piezo1-KD to control cells was calculated by dividing the percentage of the proliferating Piezo1-KD cells by the percentage of proliferating control cells in the matched donor.

TIRFM

To measure Ca^{2+} influx and the spreading of tonsillar or peripheral blood B cells on glass, PLB, or PLB-anti-Ig, live-cell Ca^{2+} signaling was imaged at 37°C and 5% CO_2 with the Nikon STORM 4 TIRF system equipped with an Apo 100× 1.49 NA TIRF objective and an Andor 512 × 512 EMCCD camera. Cells that were left untreated or were pretreated with 20 μM OB-1 for 1 hour or with 5 μM GsMTx4, 1 mM EGTA, or 1 μM P505-15 (Syk inhibitor) for 30 min at 37°C were the incubated with CAL520 for 30 min at 37°C, isolated with the

Author Manuscript Author Manuscript Author Manuscript Author Manuscript

EasySep Dead Cell Removal Kit (STEMCELL, 17899), and then stained with CellTrace Far Red cell proliferation dye according to the manufacturer's protocol. We used 488-nm and 641-nm lasers to excite emission from CAL520 and the CellTrace Far Red cell proliferation dye, respectively. Live B cells were dropped into an 18-well chambered cover glass, and time-lapse images were acquired over 15 min with no delay in the absence or presence of each inhibitor. Relative mean fluorescence intensity (MFI) values and normalized Ca^{2+} ratios were measured with in-house developed ImageJ macros and MATLAB code to track the changes in Ca^{2+} (34). Dead cells were excluded from the analysis.

FLIM

Changes in the plasma membrane tension of tonsillar or peripheral blood B cells on glass, PLB, or PLB–anti- Ig were measured by FLIM using the Zeiss LSM 780 confocal microscope equipped with a Coherent Chameleon II Ti:Sapphire femtosecond-pulsed infrared laser at 750 nm, 480/40 BFP filter, Becker and Hickl TCSPC DCC-100 control card with HCM-100 detectors and Spcm64 acquisition software, a PlanApo 63× 1.4 NA objective lens, and 37°C incubation at 5% CO_2, as previously described (54). B cells were isolated, and dead cells were further removed with the Easy-Sep Dead Cell Removal Kit before staining with the monoclonal antibody anti-CD27-BV421, a memory B cell marker, and Flipper-TR dye. Live B cells that were left untreated or were pretreated with 20 μM OB-1 were dropped into individual wells of an 18-well chambered cover glass. As cells adhered to the coverslip surface, images were captured by confocal microscopy and FLIM. SPCImage software and MATLAB (52) were used to determine the mean fluorescence lifetime values of cells from the Flipper-TR dye with code developed to perform digital image processing. Dead cells were excluded from the analysis.

Confocal microscopy

To compare the responses of tonsil B cells to membrane-bound antigen and soluble antigen in the absence or presence of OB-1, live-cell Ca^{2+} images were acquired at 37°C with a Zeiss LSM 780 confocal microscope equipped with an EC Plan-Neofluar 40×/1.3 Oil DIC M27 objective lens, 405-, 488-, and 633-nm laser excitation lines, and 37°C incubation with 5% CO_2 controlled by ZEN software (Carl Zeiss). Tonsil B cells untreated or pretreated with 20 μM OB-1 were labeled with CAL520 and then 100 nM goat polyclonal Fab fragment anti-human IgD-DyLight650 and monoclonal anti-human CD10-BV421 (at a 1:20 dilution) to discriminate non-GC B cells from naïve and memory B cells. The cells were then placed on PLB or PLB-anti-Ig on chambered cover glass in the presence or absence of OB-1, and time-lapse images were captured at 2-s intervals at 16-bit depth fluorescence intensity and at 512 × 512-pixels in size. The acquired images were background-subtracted and analyzed for MFI per cell. For the responses on PLB and PLB-anti-Ig, the fold-change in Ca^{2+} signal was calculated relative to that of B cells at the time of initial contact, whereas for the soluble antigen response, the fold-change in Ca^{2+} flux was calculated from the CAL520 MFI per cell from time-lapse images captured after adding the anti-Ig to the settled B cells relative to the value from the image before adding the antigen with ImageJ software (NIH). Dead cells were excluded from the analysis.

Author Manuscript Author Manuscript Author Manuscript Author Manuscript

Statistical analysis

Statistical significance was determined by one-sample student *t*-test with a theoretical mean of 0, two-tailed paired *t*-test, or unpaired *t*-test with Welch's correction, Mann Whitney test, or Kruskal-Wallis test followed by Dunn's multiple comparisons test as appropriate. For data that are presented as ratios or fold-changes, values were transformed to the log scale before statistical analysis. The statistical method used is indicated in the respective figure legend. $P < 0.05$ was considered as statistically significant. Prism 9 software (GraphPad) was used for all statistical analyses. The data from live-cell imaging over time were tested for statistical significance (95% confidence interval) assessed with the 'compareGrowthCurves' function from the statmod statistical modeling package (available at: http://bioinf.wehi.edu.au/software/compareCurves) available from the R Project for Statistical Computing (53).

Supplementary Material

Refer to Web version on PubMed Central for supplementary material.

Acknowledgments:

We thank R. Kissinger (NIAID) for the schematic drawing for the figure. We also thank L. Krymskaya (NIAID) at the LIG Flow Cytometry Core for assistance with flow cytometry and cell sorting.

Funding:

This work was supported by the Intramural Research Program of the NIAID, NIH.

References and Notes

1. Kwak K, Akkaya M, Pierce SK, B cell signaling in context. Nat Immunol 20, 963–969 (2019). [PubMed: 31285625]
2. Shlomchik MJ, Luo W, Weisel F, Linking signaling and selection in the germinal center. Immunological reviews 288, 49–63 (2019). [PubMed: 30874353]
3. Cyster JG, Allen CDC, B Cell Responses: Cell Interaction Dynamics and Decisions. Cell 177, 524–540 (2019). [PubMed: 31002794]
4. Kurosaki T, Shinohara H, Baba Y, B cell signaling and fate decision. Annu Rev Immunol 28, 21–55 (2010). [PubMed: 19827951]
5. Batista FD, Harwood NE, The who, how and where of antigen presentation to B cells. Nat Rev Immunol 9, 15–27 (2009). [PubMed: 19079135]
6. Tolar P, Sohn HW, Pierce SK, Viewing the antigen-induced initiation of B-cell activation in living cells. Immunological reviews 221, 64–76 (2008). [PubMed: 18275475]
7. Yuseff MI, Pierobon P, Reversat A, Lennon-Dumenil AM, How B cells capture, process and present antigens: a crucial role for cell polarity. Nat Rev Immunol 13, 475–486 (2013). [PubMed: 23797063]
8. Tolar P, Cytoskeletal control of B cell responses to antigens. Nat Rev Immunol 17, 621–634 (2017). [PubMed: 28690317]
9. Batista FD, Iber D, Neuberger MS, B cells acquire antigen from target cells after synapse formation. Nature 411, 489–494 (2001). [PubMed: 11373683]
10. Harwood NE, Batista FD, Early events in B cell activation. Annu Rev Immunol 28, 185–210 (2010). [PubMed: 20192804]

Author Manuscript Author Manuscript Author Manuscript Author Manuscript

11. Batista FD, Arana E, Barral P, Carrasco YR, Depoil D, Eckl-Dorna J, Fleire S, Howe K, Vehlow A, Weber M, Treanor B, The role of integrins and coreceptors in refining thresholds for B-cell responses. Immunological reviews 218, 197–213 (2007). [PubMed: 17624954]
12. Depoil D, Fleire S, Treanor BL, Weber M, Harwood NE, Marchbank KL, Tybulewicz VL, Batista FD, CD19 is essential for B cell activation by promoting B cell receptor-antigen microcluster formation in response to membrane-bound ligand. Nat Immunol 9, 63–72 (2008). [PubMed: 18059271]
13. Portugal S, Tipton CM, Sohn H, Kone Y, Wang J, Li S, Skinner J, Virtaneva K, Sturdevant DE, Porcella SF, Doumbo OK, Doumbo S, Kayentao K, Ongoiba A, Traore B, Sanz I, Pierce SK, Crompton PD, Malaria-associated atypical memory B cells exhibit markedly reduced B cell receptor signaling and effector function. Elife 4, (2015).
14. Ambegaonkar AA, Kwak K, Sohn H, Manzella-Lapeira J, Brzostowski J, Pierce SK, Expression of inhibitory receptors by B cells in chronic human infectious diseases restricts responses to membrane-associated antigens. Sci Adv 6, eaba6493 (2020). [PubMed: 32754637]
15. Nowosad CR, Spillane KM, Tolar P, Germinal center B cells recognize antigen through a specialized immune synapse architecture. Nat Immunol 17, 870–877 (2016). [PubMed: 27183103]
16. Coste B, Mathur J, Schmidt M, Earley TJ, Ranade S, Petrus MJ, Dubin AE, Patapoutian A, Piezo1 and Piezo2 are essential components of distinct mechanically activated cation channels. Science 330, 55–60 (2010). [PubMed: 20813920]
17. Kefauver JM, Ward AB, Patapoutian A, Discoveries in structure and physiology of mechanically activated ion channels. Nature 587, 567–576 (2020). [PubMed: 33239794]
18. Solis AG, Bielecki P, Steach HR, Sharma L, Harman CCD, Yun S, de Zoete MR, Warnock JN, To SDF, York AG, Mack M, Schwartz MA, Dela Cruz CS, Palm NW, Jackson R, Flavell RA, Mechanosensation of cyclical force by PIEZO1 is essential for innate immunity. Nature 573, 69–74 (2019). [PubMed: 31435009]
19. Jairaman A, Othy S, Dynes JL, Yeromin AV, Zavala A, Greenberg ML, Nourse JL, Holt JR, Cahalan SM, Marangoni F, Parker I, Pathak MM, Cahalan MD, Piezo1 channels restrain regulatory T cells but are dispensable for effector CD4(+) T cell responses. Sci Adv 7, (2021).
20. Hope JM, Dombroski JA, Pereles RS, Lopez-Cavestany M, Greenlee JD, Schwager SC, Reinhart-King CA, King MR, Fluid shear stress enhances T cell activation through Piezo1. BMC Biol 20, 61 (2022). [PubMed: 35260156]
21. Liu CSC, Raychaudhuri D, Paul B, Chakrabarty Y, Ghosh AR, Rahaman O, Talukdar A, Ganguly D, Cutting Edge: Piezo1 Mechanosensors Optimize Human T Cell Activation. J Immunol 200, 1255–1260 (2018). [PubMed: 29330322]
22. Fotiou E, Martin-Almedina S, Simpson MA, Lin S, Gordon K, Brice G, Atton G, Jeffery I, Rees DC, Mignot C, Vogt J, Homfray T, Snyder MP, Rockson SG, Jeffery S, Mortimer PS, Mansour S, Ostergaard P, Novel mutations in PIEZO1 cause an autosomal recessive generalized lymphatic dysplasia with non-immune hydrops fetalis. Nat Commun 6, 8085 (2015). [PubMed: 26333996]
23. Longo NS, Lugar PL, Yavuz S, Zhang W, Krijger PH, Russ DE, Jima DD, Dave SS, Grammer AC, Lipsky PE, Analysis of somatic hypermutation in X-linked hyper-IgM syndrome shows specific deficiencies in mutational targeting. Blood 113, 3706–3715 (2009). [PubMed: 19023113]
24. Wetzel C, Pifferi S, Picci C, Gok C, Hoffmann D, Bali KK, Lampe A, Lapatsina L, Fleischer R, Smith ES, Begay V, Moroni M, Estebanez L, Kuhnemund J, Walcher J, Specker E, Neuenschwander M, von Kries JP, Haucke V, Kuner R, Poulet JF, Schmoranzer J, Poole K, Lewin GR, Small-molecule inhibition of STOML3 oligomerization reverses pathological mechanical hypersensitivity. Nat Neurosci 20, 209–218 (2017). [PubMed: 27941788]
25. Bae C, Sachs F, Gottlieb PA, The mechanosensitive ion channel Piezo1 is inhibited by the peptide GsMTx4. Biochemistry 50, 6295–6300 (2011). [PubMed: 21696149]
26. Depoil D, Weber M, Treanor B, Fleire SJ, Carrasco YR, Harwood NE, Batista FD, Early events of B cell activation by antigen. Sci Signal 2, pt1 (2009). [PubMed: 19318623]
27. Lewis AH, Grandl J, Mechanical sensitivity of Piezo1 ion channels can be tuned by cellular membrane tension. Elife 4, (2015).
28. Guo YR, MacKinnon R, Structure-based membrane dome mechanism for Piezo mechanosensitivity. Elife 6, (2017).

Author Manuscript Author Manuscript Author Manuscript Author Manuscript

29. Lin YC, Guo YR, Miyagi A, Levring J, MacKinnon R, Scheuring S, Force-induced conformational changes in PIEZO1. Nature 573, 230–234 (2019). [PubMed: 31435018]
30. Colom A, Derivery E, Soleimanpour S, Tomba C, Molin MD, Sakai N, Gonzalez-Gaitan M, Matile S, Roux A, A fluorescent membrane tension probe. Nat Chem 10, 1118–1125 (2018). [PubMed: 30150727]
31. Goujon A, Colom A, Strakova K, Mercier V, Mahecic D, Manley S, Sakai N, Roux A, Matile S, Mechanosensitive Fluorescent Probes to Image Membrane Tension in Mitochondria, Endoplasmic Reticulum, and Lysosomes. J Am Chem Soc 141, 3380–3384 (2019). [PubMed: 30744381]
32. Wang Y, Chi S, Guo H, Li G, Wang L, Zhao Q, Rao Y, Zu L, He W, Xiao B, A lever-like transduction pathway for long-distance chemical- and mechano-gating of the mechanosensitive Piezo1 channel. Nature Communications 9, 1300 (2018).
33. Botello-Smith WM, Jiang W, Zhang H, Ozkan AD, Lin YC, Pham CN, Lacroix JJ, Luo Y, A mechanism for the activation of the mechanosensitive Piezo1 channel by the small molecule Yoda1. Nat Commun 10, 4503 (2019). [PubMed: 31582801]
34. Kwak K, Quizon N, Sohn H, Saniee A, Manzella-Lapeira J, Holla P, Brzostowski J, Lu J, Xie H, Xu C, Spillane KM, Tolar P, Pierce SK, Intrinsic properties of human germinal center B cells set antigen affinity thresholds. Sci Immunol 3, (2018).
35. Liu W, Chen E, Zhao XW, Wan ZP, Gao YR, Davey A, Huang E, Zhang L, Crocetti J, Sandoval G, Joyce MG, Miceli C, Lukszo J, Aravind L, Swat W, Brzostowski J, Pierce SK, The scaffolding protein synapse-associated protein 97 is required for enhanced signaling through isotype-switched IgG memory B cell receptors. Sci Signal 5, ra54 (2012). [PubMed: 22855505]
36. Lopez-Cabrera M, Santis AG, Fernandez-Ruiz E, Blacher R, Esch F, Sanchez-Mateos P, Sanchez-Madrid F, Molecular cloning, expression, and chromosomal localization of the human earliest lymphocyte activation antigen AIM/CD69, a new member of the C-type animal lectin superfamily of signal-transmitting receptors. J Exp Med 178, 537–547 (1993). [PubMed: 8340758]
37. Douguet D, Honore E, Mammalian Mechanoelectrical Transduction: Structure and Function of Force-Gated Ion Channels. Cell 179, 340–354 (2019). [PubMed: 31585078]
38. Zheng W, Sachs F, Investigating the structural dynamics of the PIEZO1 channel activation and inactivation by coarse-grained modeling. Proteins 85, 2198–2208 (2017). [PubMed: 28905417]
39. De Vecchis D, Beech DJ, Kalli AC, Molecular dynamics simulations of Piezo1 channel opening by increases in membrane tension. Biophys J 120, 1510–1521 (2021). [PubMed: 33582135]
40. Cox CD, Bae C, Ziegler L, Hartley S, Nikolova-Krstevski V, Rohde PR, Ng CA, Sachs F, Gottlieb PA, Martinac B, Removal of the mechanoprotective influence of the cytoskeleton reveals PIEZO1 is gated by bilayer tension. Nat Commun 7, 10366 (2016). [PubMed: 26785635]
41. Tolar P, Hanna J, Krueger PD, Pierce SK, The constant region of the membrane immunoglobulin mediates B cell-receptor clustering and signaling in response to membrane antigens. Immunity 30, 44–55 (2009). [PubMed: 19135393]
42. Sohn HW, Gu H, Pierce SK, Cbl-b negatively regulates B cell antigen receptor signaling in mature B cells through ubiquitination of the tyrosine kinase Syk. J Exp Med 197, 1511–1524 (2003). [PubMed: 12771181]
43. Schiller J, Lowy D, Explanations for the high potency of HPV prophylactic vaccines. Vaccine 36, 4768–4773 (2018). [PubMed: 29325819]
44. Ma S, Cahalan S, LaMonte G, Grubaugh ND, Zeng W, Murthy SE, Paytas E, Gamini R, Lukacs V, Whitwam T, Loud M, Lohia R, Berry L, Khan SM, Janse CJ, Bandell M, Schmedt C, Wengelnik K, Su AI, Honore E, Winzeler EA, Andersen KG, Patapoutian A, Common PIEZO1 Allele in African Populations Causes RBC Dehydration and Attenuates Plasmodium Infection. Cell 173, 443–455 e412 (2018). [PubMed: 29576450]
45. Crompton PD, Moebius J, Portugal S, Waisberg M, Hart G, Garver LS, Miller LH, Barillas-Mury C, Pierce SK, Malaria immunity in man and mosquito: insights into unsolved mysteries of a deadly infectious disease. Annu Rev Immunol 32, 157–187 (2014). [PubMed: 24655294]
46. Ambegaonkar AA, Nagata S, Pierce SK, Sohn H, The Differentiation in vitro of Human Tonsil B Cells With the Phenotypic and Functional Characteristics of T-bet+ Atypical Memory B Cells in Malaria. Front Immunol 10, 852 (2019). [PubMed: 31068937]

Author Manuscript Author Manuscript Author Manuscript Author Manuscript

47. Lock JT, Parker I, Smith IF, A comparison of fluorescent Ca(2)(+) indicators for imaging local Ca(2)(+) signals in cultured cells. Cell Calcium 58, 638–648 (2015). [PubMed: 26572560]

48. Weaver GC, Villar RF, Kanekiyo M, Nabel GJ, Mascola JR, Lingwood D, In vitro reconstitution of B cell receptor-antigen interactions to evaluate potential vaccine candidates. Nat Protoc 11, 193–213 (2016). [PubMed: 26741406]

49. Livak KJ, Schmittgen TD, Analysis of relative gene expression data using real-time quantitative PCR and the 2(-Delta Delta C(T)) Method. Methods 25, 402–408 (2001). [PubMed: 11846609]

50. Gudipaty SA, Lindblom J, Loftus PD, Redd MJ, Edes K, Davey CF, Krishnegowda V, Rosenblatt J, Mechanical stretch triggers rapid epithelial cell division through Piezo1. Nature 543, 118–121 (2017). [PubMed: 28199303]

51. Sohn HW, Tolar P, Brzostowski J, Pierce SK, A method for analyzing protein-protein interactions in the plasma membrane of live B cells by fluorescence resonance energy transfer imaging as acquired by total internal reflection fluorescence microscopy. Methods Mol Biol 591, 159–183 (2010). [PubMed: 19957130]

52. Manzella-Lapeira J, Brzostowski J, Fluorescence Lifetime Imaging as a Noninvasive Tool to Study Plasmodium Falciparum Metabolism. Methods Mol Biol 2304, 301–313 (2021). [PubMed: 34028724]

53. Davey AM, Pierce SK, Intrinsic differences in the initiation of B cell receptor signaling favor responses of human IgG(+) memory B cells over IgM(+) naive B cells. J Immunol 188, 3332–3341 (2012). [PubMed: 22379037]

Author Manuscript Author Manuscript Author Manuscript Author Manuscript

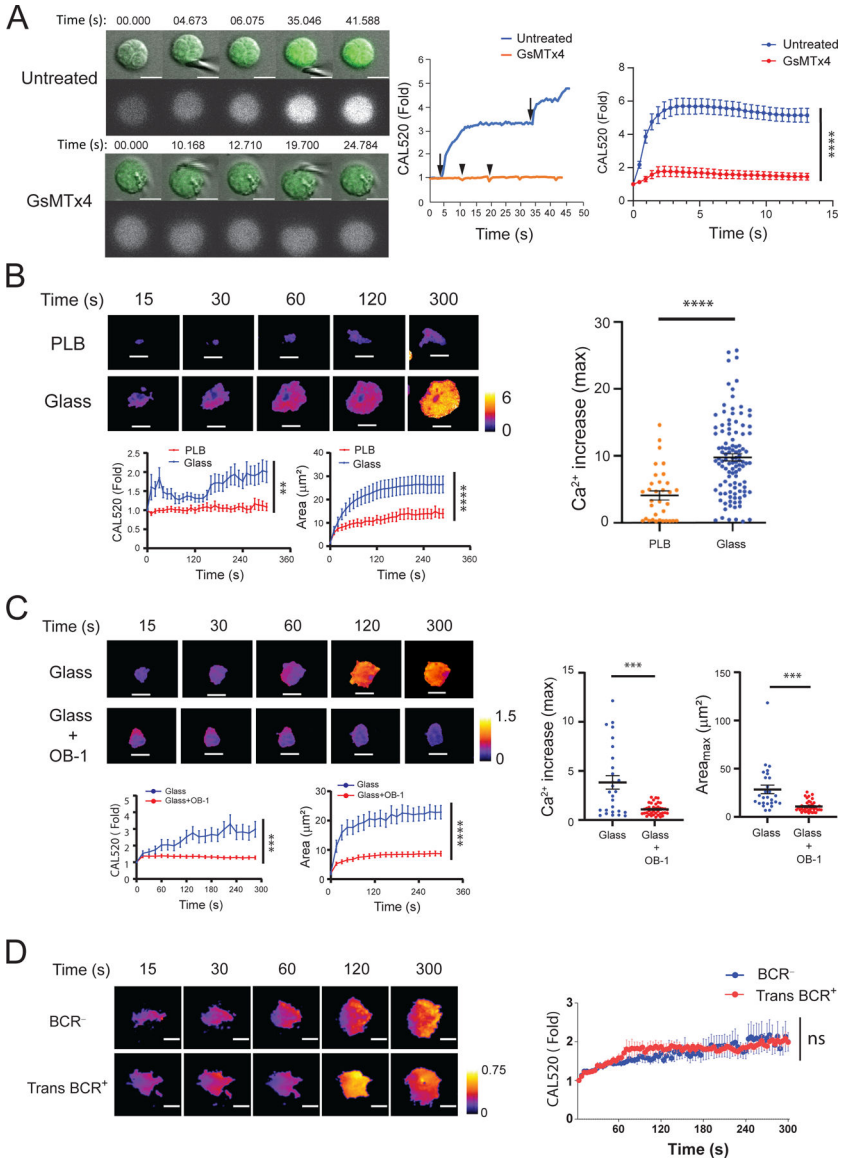

Fig. 1. B cells flux Ca^{2+} in response to touch in a Piezo1-dependent manner.

(**A**) Purified human peripheral blood or tonsillar naive B cells were loaded with the Ca^{2+} indicator dye, CAL520, and placed in a glass chamber for 5 to 30 min, in the absence (Untreated) or presence of the Piezo1 inhibitor, GsMTx4. The cells were then touched with a glass probe and images were captured by confocal microscopy. Left: Images of the Ca^{2+} signals of two representative cells that were either untreated or treated with GsMTx4 before, during, and after contact with the glass probe. Middle: Quantification of the fold-increase in Ca^{2+} flux for each of the cells over the course of 40 s. Right: The average fold-change in Ca^{2+} flux (relative to that in cells at the time of first contact) in untreated B cells (36 cells) and GsMTx4-treated B cells (54 cells) over 13 s. Data are means ± SEM from three experiments. (**B**) Purified human tonsillar $CD10^{-}$ naïve and memory B cells were loaded with CAL520 and a red fluorescent dye as an indicator of cell volume and were placed on a planar lipid bilayer (PLB) or glass coverslips (Glass) and imaged over time by TIRFM. Top:

Author Manuscript Author Manuscript Author Manuscript Author Manuscript

Representative images of two B cells placed on PLB or glass and displayed as color-coded ratio images by normalizing CAL520 MFI with red fluorescence dye MFI and quantification of Ca^{2+} fluxes and contact areas with time after first contact with the PLB (26 cells) or glass (36 cells). Bottom: The fold-change in Ca^{2+} flux over time relative to the first point of contact of the cell with glass or PLB (left) and the area of contact of the indicated cells with the surface over time (right). Right: Comparison of the maximal Ca^{2+} flux increases of cells placed on PLB or glass, which were calculated for each cell by normalizing its maximal CAL520 MFI to the MFI upon first contact with PLB (33 cells) or glass (110 cells). Data are means ± SEM from one experiment that is representative of six experiments. (**C**) Tonsillar naïve B cells and memory B cells were left untreated or were pretreated with 20 μM OB-1 and analyzed by TIRFM on glass in the continued presence of OB-1. Left: Representative images of two cells (top) and quantification of changes in Ca^{2+} flux (bottom left) and cell area (bottom right) over time. Right: Comparison of the maximal Ca^{2+} flux increases and maximal area of cell spreading ($Area_{max}$) for cells placed on glass in the absence (27 cells) or presence (39 cells) of OB-1. Data are means ± SEM from one experiment that is representative of 11 experiments. (**D**) BCR^- Ramos cells or Ramos cells transduced to stably express exogeneous IgM H and L chain (Trans BCR^+) were loaded with CAL520 and red fluorescence dye and placed on glass for the indicated times while Ca^{2+} flux were recorded. Representative ratio images (left) and quantification of fold-change in Ca^{2+} flux for BCR^- cells (31 cells) and Trans BCR^+ cells (30 cells) over time. Data are means ± SEM from one experiment that is representative of three experiments. Scale bars, 5 μm. (B to D) Scale ranges of the 8-bit, color-coded image display. The kinetic data in (A) to (D) were tested for statistical significance (95% confidence interval) with the 'compareGrowthCurves' function (see Materials and Methods). $^{**}P \leq 0.01$, $^{***}P \leq 0.001$, and $^{****}P \leq 0.0001$; ns, not significant. For (B and C, right), data were analyzed by two-tailed unpaired *t*-test with Welch's correction. $^{***}P \leq 0.001$ and $^{****}P \leq 0.0001$.

Author Manuscript Author Manuscript Author Manuscript Author Manuscript

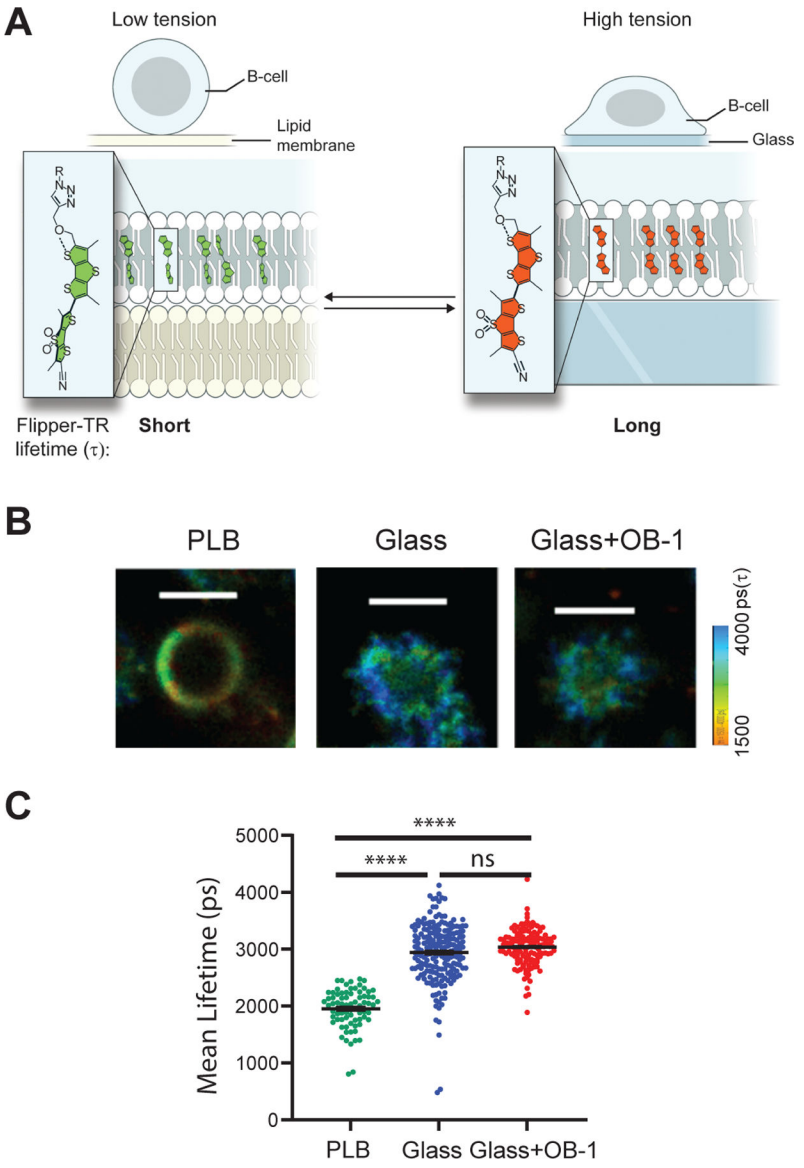

Fig. 2. Plasma membrane tension is increases in B cells placed on glass surfaces.

(**A**) A schematic depiction of the tension probe, Flipper-TR, when intercalated into the plasma membranes of B cells placed on PLB, which exerts low tension (left), or on glass, which exerts high tension (right). The fluorescence lifetime of Flipper-TR is determined by FLIM imaging and calculated as fluorescence lifetime decay (**τ**). Flipper-TR has a short lifetime under low membrane tension and a long lifetime under high membrane tension. (**B**) Tonsillar naive B cells and memory B cells were untreated or pretreated with OB-1, labeled with Flipper-TR, washed, and placed on PLB (for untreated cells) or on glass (for untreated and OB-1–treated cells) and imaged by FLIM with a ZEISS 780 confocal microscope equipped with FLIM apparatus. Scale bars, 5 μm. Color-coded scale range is given. (C) Flipper-TR mean lifetime decay rate (**τ**) was calculated per cell under the indicated conditions with MATLAB code. Data are means ± SEM from five independent experiments and were tested by nested, one-way ANOVA. ****$P \leq 0.0001$; ns, $P > 0.05$.

Author Manuscript Author Manuscript Author Manuscript Author Manuscript

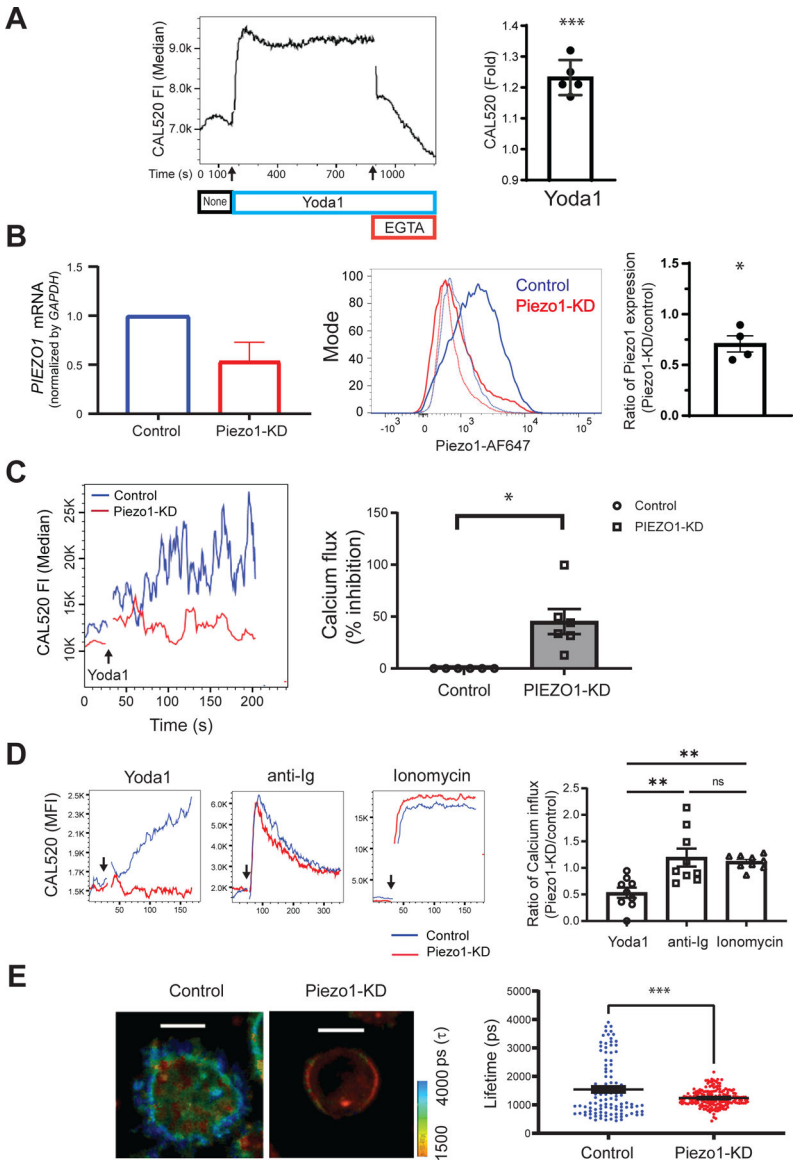

Fig. 3. siRNA-mediated knockdown of Piezo1 inhibits B cell responses.

(**A**) Purified human tonsillar B cells were labeled with CAL520 and a monoclonal antibody specific for the GC B cell marker, CD10, to gate naïve and memory B cells. After 180 s of baseline recording (None, black), 15 μM Yoda1 (blue) was added to the B cells in solution, which was followed by the addition of 2 mM EGTA (red). Ca^{2+} signals were analyzed for 1200 s by flow cytometry. Left: Representative plot of the median CAL520 fluorescence intensity (FI) values over time. Right: Quantification of the Ca^{2+} influxes calculated for B cells from five donors as the fold-change in the median CAL520 FI induced by Yoda-1 relative to the baseline FI. Data are means ± SEM from five independent experiments. (**B**) B cells purified from human PBMCs with magnetic beads were transfected with either control siRNA (Control) or Piezo1-specific siRNA (Piezo1-KD) with a 4D Amaxa nucleofector. Left: *PIEZO1* mRNA abundance was quantified by real-time qRT-PCR analysis and normalized to that of *GAPDH* mRNA. Middle: Representative histogram of total Piezo1

Author Manuscript Author Manuscript Author Manuscript Author Manuscript

abundance by flow cytometry after immunofluorescence staining with an Alexa Fluor 647–labeled Piezo-specific antibody. Right: Quantification of Piezo1 abundance for B cells from four donors shown as the ratio of the Piezo1 abundance in Piezo1-KD cells relative to that in Control cells. Data are means ± SEM from four independent experiments. (**C**) Control and Piezo1-KD B cells were labeled with CAL520 and Ca^{2+} flux was measured over time by flow cytometry before and after the addition of 15 μM Yoda-1. Left: Representative Ca^{2+} curves after Yoda-1 treatment of the indicate cells. Right: Quantification of the percentage inhibition of the Ca^{2+} flux in Piezo1-KD cells as compared to that in Control cells obtained from six donors. Data are means ± SEM from six independent experiments. (**D**) Control and Piezo1-KD B cells were labeled with CAL520, and Ca^{2+} fluxes were measured over time by flow cytometry for cells treated with Yoda-1, anti-Ig, or ionomycin. Left: Representative Ca^{2+} kinetics plot with arrows marking the times, after baseline recording, when each stimulant was added. Right: Quantification of Ca^{2+} increases induced by Yoda1, soluble anti-Ig, or ionomycin were calculated as the ratio of the fold-changes in CAL520 MFI between Piezo1-KD and Control cells upon stimulation relative to the baseline MFI for B cells from nine donors. Data are means ± SEM from nine independent experiments. (**E**) Control and Piezo1-KD B cells were labeled with Flipper-TR and placed on glass and the lifetime decay of the dye was determined. Left: Two representative B cells showing lifetime decay. Right: Quantification of the lifetime decay of Flipper-TR for control (111 cells) and Piezo1-KD (177 cells) B cells. Scale bars, 5 μm. Data are means ± SEM from five independent experiments. $*P \leq 0.05$, $**P \leq 0.01$, and $***P \leq 0.001$; ns, not significant. Data in (A) to (C) were analyzed by one-sample *t* test with a hypothetical value of zero, data in (D) were analyzed by Kruskal-Wallis test, followed by Dunn's multiple comparisons test; and data in (E) were analyzed by two-tailed, unpaired *t* test with Welch's correction.

Author Manuscript Author Manuscript Author Manuscript Author Manuscript

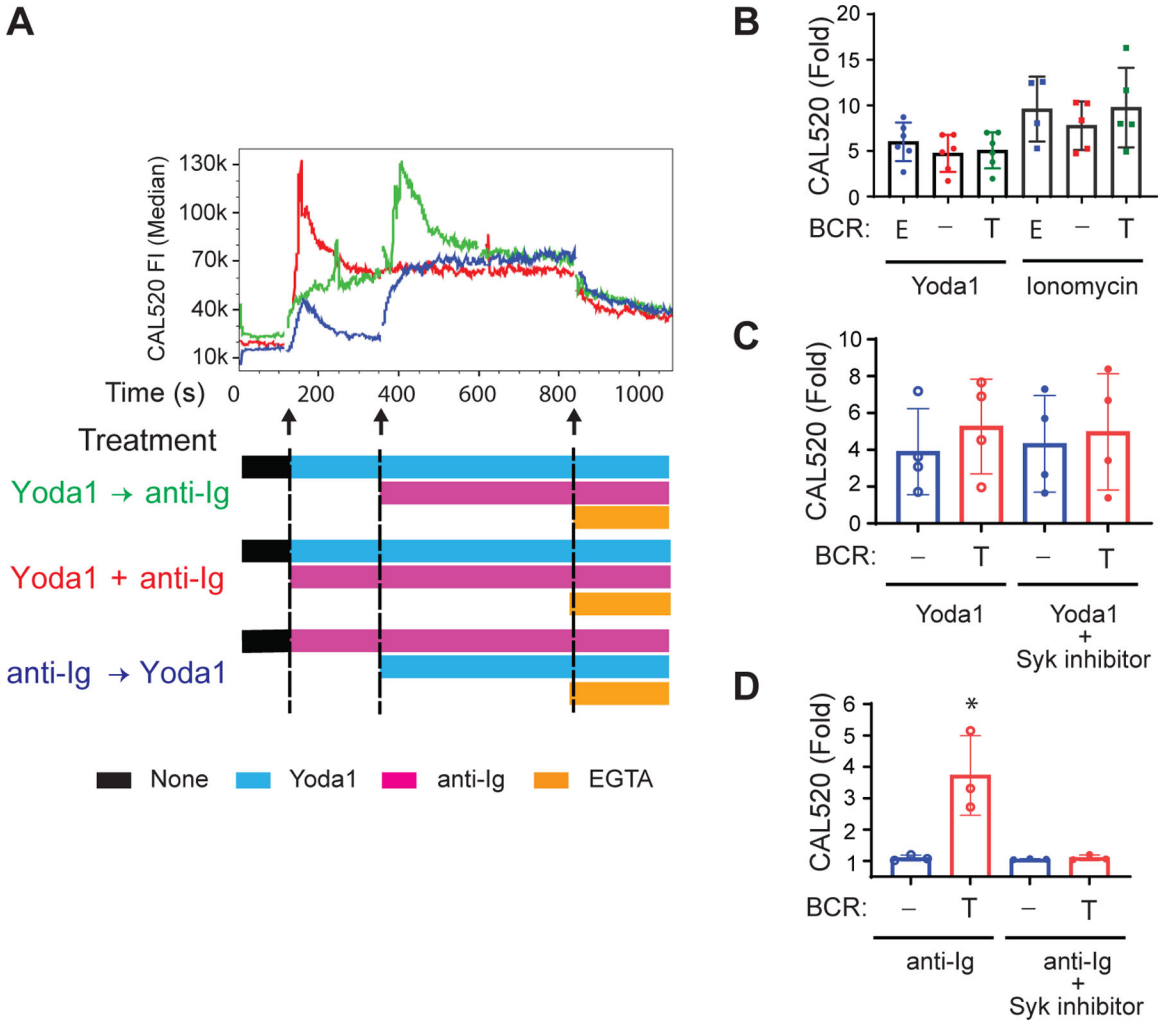

Fig. 4. The Piezo1 agonist Yoda1 and BCR-crosslinking stimulate independent Ca^{2+} fluxes in B cells.

(**A**) Naïve B cells and memory B cells in solution were incubated with mouse monoclonal antibody (10 μg/ml) specific for human κ light chain (anti-Ig) as a surrogate soluble antigen after Yoda1 addition (Yoda1 → anti-Ig) simultaneously with Yoda1 (Yoda1 + anti-Ig), or before Yoda1 (anti-Ig → Yoda1), as indicated. Median Ca^{2+} fluxes are representative of three independent experiments. (**B** to **D**) Ramos cells expressing an endogenous μ HC and λ LC indicated as 'E,' no BCR, indicated as '−,' or transduced to stably express a Trans BCR, indicated as 'T,' were labeled with CAL520 and Ca^{2+} flux was recorded by flow cytometry before and after the addition of Yoda1 or ionomycin (B), Yoda1 alone or with 1.0 μM P505-15 (C), or anti-Ig alone or with 1.0 μM P505-15 (D). The fold-change in CAL520 MFI relative to the baseline was calculated from MFIs for the baseline (50 s), Yoda-1 (180 s), or ionomycin (120 s), or from the peak MFI for soluble anti-Ig (300 s). Data are means ± SEM from more than four (B and C) and three (D) independent experiments. *$P < 0.05$ as determined by two-tailed, unpaired *t* test with Welch's correction between BCR^{-} and Trans BCR cells and two-tailed, paired *t* test between anti-Ig and anti-Ig + P505-15.

Author Manuscript Author Manuscript Author Manuscript Author Manuscript

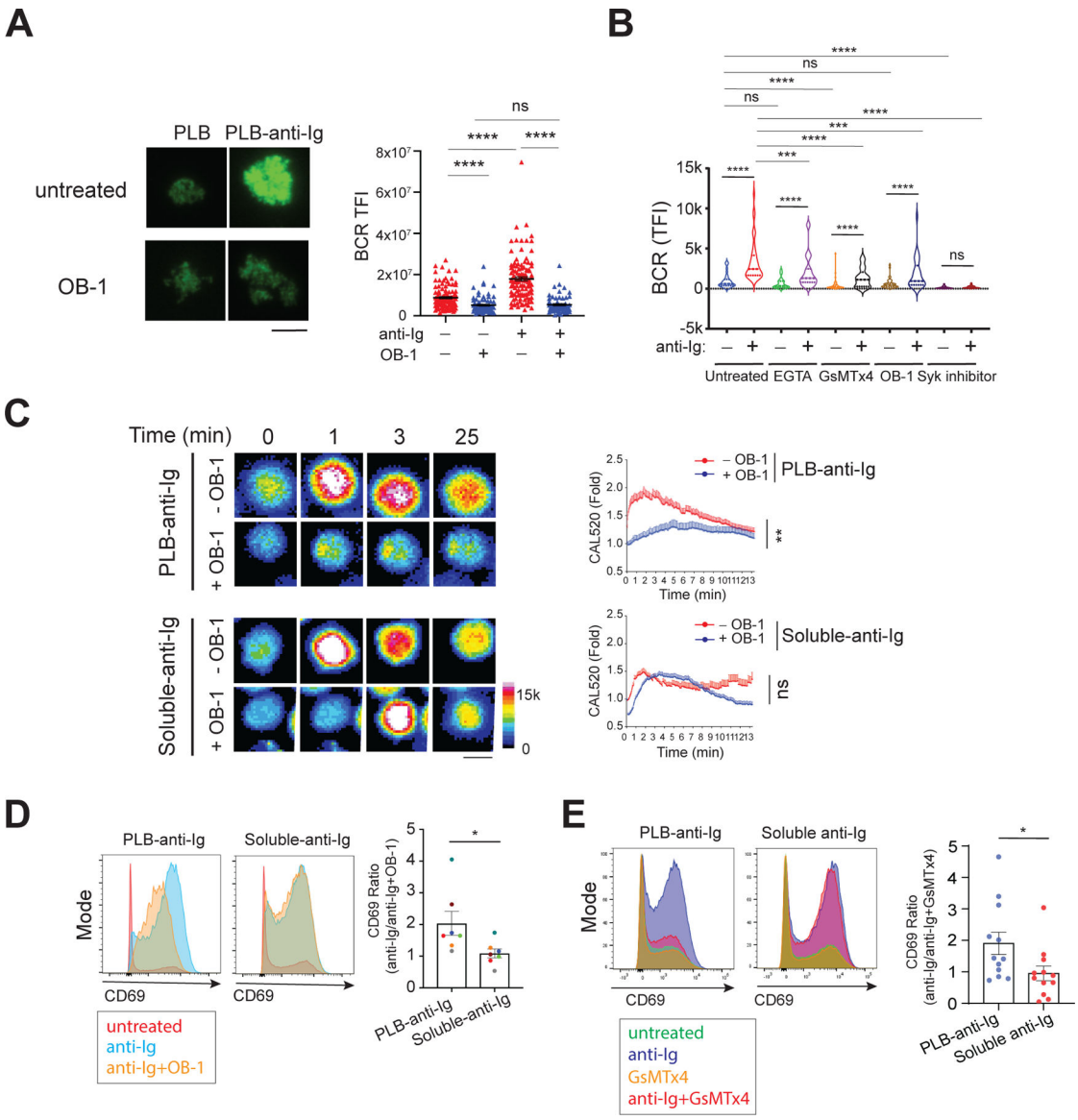

Fig. 5. Piezo1 is required for B cell responses to membrane-associated, but not soluble, anti-Ig.

(**A**) Naive B cells were labeled with fluorescently conjugated Fab anti-human IgM to label the BCR. Cells were placed on PLB alone or on PLB attached to anti-Ig for 25 min at 37°C in the absence or presence of OB-1, and images were obtained by TIRFM. Left: Representative images of BCR recruited to the contact area of four cells placed on PLB or PLB–anti-Ig acquired with a 16-bit scale. Right: Quantification of the total fluorescence intensity (TFI) of the BCRs in the contact area with the PLB for >60 cells per condition. Data are means ± SEM from two independent experiments. Scale bar, 5 μm. (**B**) Tonsillar naive and memory B cells isolated by negative selection with CD10 beads were labeled with a mixture of Alexa Fluor 647–conjugated goat Fab anti-human IgM and Fab anti-human IgG, placed on PLB or PLB–anti-Ig in the absence or presence of 1 mM EGTA, 5 μM GsMTx4, 20 μM OB-1, or 1 μM P505–15 (Syk inhibitor) for 20 min and fixed. Images were obtained by TIRFM and the TFI values of the BCR recruited to the

Author Manuscript Author Manuscript Author Manuscript Author Manuscript

cell contact area were quantified with ImageJ software for >30 cells per condition from three independent experiments. (**C**) Untreated or OB-1–pretreated naïve B cells were labeled with CAL520 and Ca^{2+} fluxes were imaged with a ZEISS 780 confocal microscope upon B cell contact with PLB–anti-Ig or after the addition of anti-Ig to B cells settled on PLB (soluble-anti-Ig) in the absence or presence of 20 μM OB-1. Left: Representative CAL520 images of four cells at the indicated times displayed as color-coded images. Scale bars, 5 μm. Intensity ranges are given. Right: The Ca^{2+} fluxes were quantified and are presented as the fold-increase relative to the signal of resting cells for B cells placed on PLB-anti-Ig in the presence (29 cells) or absence (38 cells) of OB-1 and for B cells stimulated with soluble anti-Ig in the presence (57 cells) or absence (36 cells) of OB-1. Data are means ± SEM from two independent experiments. (**D** and **E**) Naïve and memory B cells were incubated overnight with PLB–anti-Ig or soluble anti-Ig in the presence or absence of OB-1 (D) or GsMTx4 (E). Left: Representative flow cytometry plots of cell surface CD69 expression. Right: Quantification of the ratio of the abundance of CD69 expressed by B cells stimulated by PLB–anti-Ig or by soluble anti-Ig in the absence of OB-1 to that of stimulated cells in the presence of OB-1. Data are means ± SEM from seven donors in three independent experiments (D) or from 12 donors in five independent experiments (E). *$P \leq 0.05$, **$P \leq 0.01$, and ****$P \leq 0.0001$; ns, $P > 0.05$. Data in (A) were analyzed by two-tailed unpaired *t* test with Welch's correction; data in (B) were analyzed by paired *t* test; data in (C) were analyzed with the 'compareGrowthCurves' function; and data in (D) and (E) were analyzed by two-tailed Mann-Whitney test.

Author Manuscript Author Manuscript Author Manuscript Author Manuscript

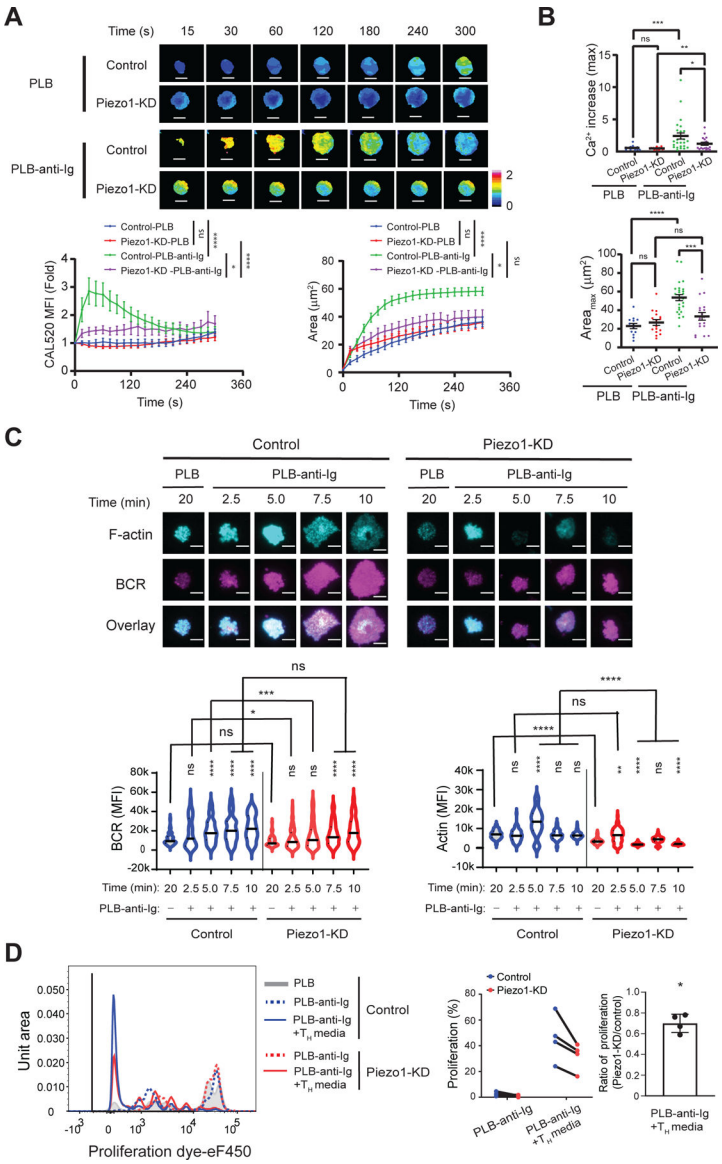

Fig. 6. The siRNA-mediated reduction in Piezo1 abundance inhibits B cell responses to PLB–anti-Ig.

(**A**) Control and Piezo1-KD B cells were loaded with CAL520 and a red fluorescent dye, placed on PLB or PLB–anti-Ig, and Ca^{2+} fluxes were imaged at 37°C by TIRFM. Top: Representative images of color-coded Ca^{2+} signals normalized by cell volume for one representative cell for each condition. Bottom: Quantification of the dynamics of the Ca^{2+} fluxes (left) and contact areas (right) for Control B cells (13 cells) and Piezo1-KD cells (16 cells) placed on PLB and Control cells (26 cells) and Piezo1-KD cells (18 cells) placed on PLB-anti-Ig. Scale bars, 5 μm. Scale ranges are provided. Data are means ± SEM from five independent experiments. $*P \leq 0.05$ and $****P \leq 0.0001$ as assessed by the 'compareGrowthCurves' function test. (**B**) Maximal Ca^{2+} increase (top) and maximal area ($Area_{max}$, bottom) were determined by calculating the fold-differences in the Ca^{2+} signal at the point of first contact with the PLB and at the point of maximal Ca^{2+} signal and contact area achieved during a 5-min incubation. $*P \leq 0.05$, $**P \leq 0.01$, $***P \leq 0.001$,

Author Manuscript Author Manuscript Author Manuscript Author Manuscript

and ****$P \leq 0.0001$; ns, $P > 0.05$. Data were analyzed by two-tailed, unpaired *t* test with Welch's correction between Control and Piezo1-KD cells and by two-tailed, paired *t* test between PLB and PLB-anti-Ig. Data are representative of four independent experiments. (**C**) BCR and F-actin recruitment to the contact area imaged by TIRFM. Control and Piezo1-KD cells labeled with Alexa Fluor 488–conjugated Fab goat anti-human IgM and IgG HC were placed on either PLB or PLB-anti-Ig for the indicted times. Fixed cells were stained with Phalloidin–Alexa Fluor 647 and imaged by TIRFM. Top: Representative images of BCR and F-actin recruited to the contact area at the indicated times for Control and Piezo1-KD cells. Bottom: Quantification of BCR (left) and F-actin (right) recruitment to the contact areas from the images for >70 cells per condition from three independent experiments. *$P \leq 0.05$, **$P \leq 0.01$, ***$P \leq 0.001$, and ****$P \leq 0.0001$ by Kruskal-Wallis test followed by Dunn's multiple comparison tests between PLB and PLB-anti-Ig at the indicated times, as well as between Control and Piezo1-KD cells; ns, $P > 0.05$. (**D**) Control and Piezo1-KD cells were cultured for 24 hours, labeled with the cell proliferation dye, eF450, and then cultured for 5 days in chambers with PLB or PLB–anti-Ig in the absence or presence of T_H medium containing anti-CD40 antibodies, IL-21, and IL-4. Left: Representative histogram of proliferation dye for each stimulation condition in Control and Piezo1-KD cells. Right: Quantification of the percentage of proliferating cells (symbol and line graph with matched donor) and the ratio of the percentage proliferation in the Piezo1-KD cells relative to that in Control cells in the same donor. Data are means ± SEM from four donors in three independent experiments. *$P \leq 0.05$ as tested by one-sample *t* test with a theoretical mean of zero.